AD-A039 382 ANALYTICAL METHODS INC BELLEVUE WASH F/G 20/4
INVESTIGATION OF THREE-DIMENSIONAL FLOW SEPARATION ON FUSELAGE --ETC(U)
MAR 77 F A DVORAK, B MASKEW, F A WOODWARD DAAJ02-75-C-0036
UNCLASSIFIED USAAMRDL-TR-77-4 NL

1 OF 1
ADA
039382

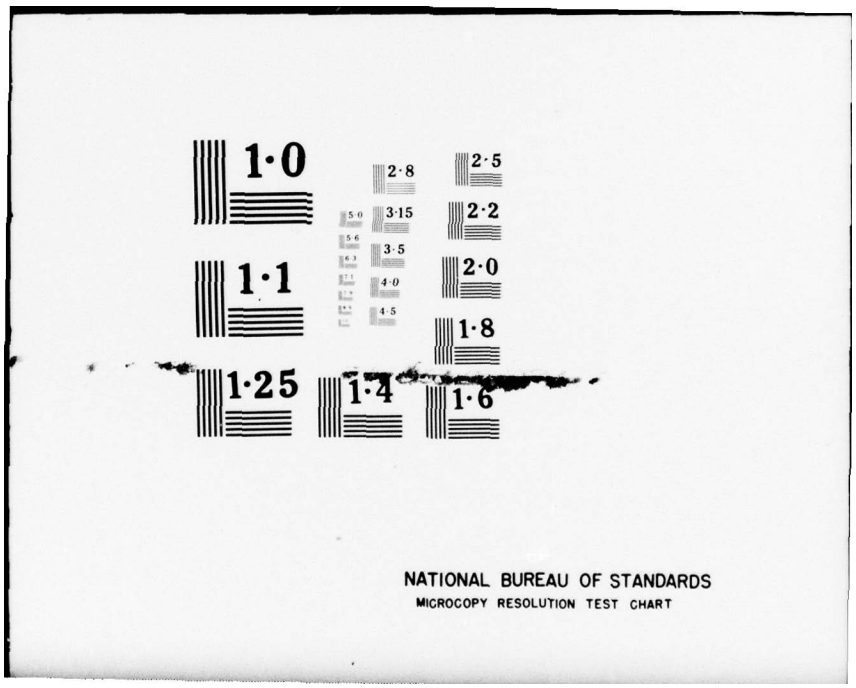
1·0
1·1
1·25
1·4
1·6
1·8
2·0
2·2
2·5
2·8
3·15
3·5
4·0
4·5
5·0
5·6
NATIONAL BUREAU OF STANDARDS
MICROCOPY RESOLUTION TEST CHART

USAAMRDL-TR-77-4

INVESTIGATION OF THREE-DIMENSIONAL FLOW SEPARATION ON FUSELAGE CONFIGURATIONS

Analytical Methods, Inc.
100 - 116th Avenue S.E.
Bellevue, Wash. 98004

March 1977

Final Report for Period May 1975 - May 1976

Approved for public release; distribution unlimited.

Prepared for

EUSTIS DIRECTORATE
U. S. ARMY AIR MOBILITY RESEARCH AND DEVELOPMENT LABORATORY
Fort Eustis, Va. 23604

EUSTIS DIRECTORATE POSITION STATEMENT

This report has been reviewed by the Eustis Directorate, U. S. Army Air Mobility Research and Development Laboratory, and is considered to be technically sound. The purpose of the research was to develop a method for predicting pressure distributions in separated flow regions on three-dimensional bodies such as helicopter fuselage configurations. The report is published for the exchange of information and appropriate application. The technical monitor for this contract was Mr. William D. Vann, Aeromechanics Technical Area, Technology Applications Division.

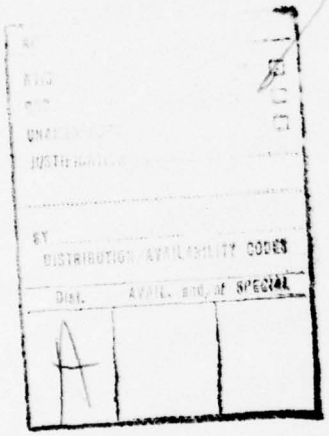

DISCLAIMERS

The findings in this report are not to be construed as an official Department of the Army position unless so designated by other authorized documents.

When Government drawings, specifications, or other data are used for any purpose other than in connection with a definitely related Government procurement operation, the United States Government thereby incurs no responsibility nor any obligation whatsoever; and the fact that the Government may have formulated, furnished, or in any way supplied the said drawings, specifications, or other data is not to be regarded by implication or otherwise as in any manner licensing the holder or any other person or corporation, or conveying any rights or permission, to manufacture, use, or sell any patented invention that may in any way be related thereto.

Trade names cited in this report do not constitute an official endorsement or approval of the use of such commercial hardware or software.

DISPOSITION INSTRUCTIONS

Destroy this report when no longer needed. Do not return it to the originator.

Unclassified

SECURITY CLASSIFICATION OF THIS PAGE (When Data Entered)

REPORT DOCUMENTATION PAGE

READ INSTRUCTIONS BEFORE COMPLETING FORM

1. REPORT NUMBER: USAAMRDL-TR-77-4	2. GOVT ACCESSION NO.
3. RECIPIENT'S CATALOG NUMBER	
4. TITLE (and Subtitle): INVESTIGATION OF THREE-DIMENSIONAL FLOW SEPARATION ON FUSELAGE CONFIGURATIONS	5. TYPE OF REPORT & PERIOD COVERED: FINAL REPORT, May 1975 - May 1976
	6. PERFORMING ORG. REPORT NUMBER
7. AUTHOR(s): Frank A. Dvorak, Brian Maskew, Frank A. Woodward	8. CONTRACT OR GRANT NUMBER(s): DAAJ02-75-C-0036
9. PERFORMING ORGANIZATION NAME AND ADDRESS: Analytical Methods, Inc., 100 - 116th Avenue S.E., Bellevue, Washington 98004	10. PROGRAM ELEMENT, PROJECT, TASK AREA & WORK UNIT NUMBERS: 62209A, 1F262209AH76, 00, 085, EK
11. CONTROLLING OFFICE NAME AND ADDRESS: Eustis Directorate, U.S. Army Air Mobility R & D Laboratory, Ft. Eustis, Virginia 23604	12. REPORT DATE: March 1977
	13. NUMBER OF PAGES: 95
14. MONITORING AGENCY NAME & ADDRESS (If different from Controlling Office)	15. SECURITY CLASS. (of this report): Unclassified
	15a. DECLASSIFICATION/DOWNGRADING SCHEDULE

16. DISTRIBUTION STATEMENT (of this Report)

Approved for public release; distribution unlimited.

17. DISTRIBUTION STATEMENT (of the abstract entered in Block 20, if different from Report)

18. SUPPLEMENTARY NOTES

19. KEY WORDS (Continue on reverse side if necessary and identify by block number)

Three Dimensional
Bodies/Fuselages
Separation
Turbulent Boundary Layer
Sources/Vortices
Wake Modeling

20. ABSTRACT (Continue on reverse side if necessary and identify by block number)

A method is described for calculating the complete pressure distribution on a body with separated flow. The boundary layer characteristics are calculated along several streamlines up to the point where separation is predicted. The separated flow is modeled by streamwise panels of uniform vorticity attached to the body near the predicted separation line. Comparisons are presented of calculated and experimental pressure distributions for a cylinder, a sphere and the BO105 fuselage. The results are in fair agreement, but there are certain features of the results and restrictions of the source/vortex inviscid model which need improvement.

DD FORM 1 JAN 73 1473 EDITION OF 1 NOV 65 IS OBSOLETE

Unclassified

SECURITY CLASSIFICATION OF THIS PAGE (When Data Entered)

392 078

PREFACE

This program was sponsored by the Eustis Directorate, U. S. Army Air Mobility Research and Development Laboratory, and was monitored by Mr. W.D. Vann. This program was authorized by Contract DAAJ02-75-C-0036.

The authors wish to thank Mr. E.W. Geller for his valuable contribution to the development of the two-dimensional separation model.

TABLE OF CONTENTS

TABLE OF CONTENTS

TABLE OF CONTENTS (continued)

LIST OF ILLUSTRATIONS

LIST OF ILLUSTRATIONS (continued)

INTRODUCTION

BACKGROUND

Until recently, the aerodynamic analysis of helicopter configurations has been largely neglected, with the exception being the analysis of rotor systems. Even in this area, a particular rotor airfoil cross-section is the result of many hours of exhaustive wind tunnel testing, usually with only a minimal amount of theoretical support. This pattern in changing, however, due to a demand for greater vehicle performance, either in speed, lifting capacity or endurance. Another consideration, the more efficient use of energy, has further altered the traditional view of helicopter aerodynamicists. Drag has become an important issue, and work is now under way on several fronts in an attempt to understand and subsequently reduce its effect through improved helicopter design.

The analysis of current helicopter fuselage designs is basically a problem in the calculation of three-dimensional bluff body aerodynamics. Flow separation results in a flow field problem which, while not necessarily intractable, remains one of the most challenging of fluid dynamic phenomena. Recourse to the wind tunnel is only moderately successful because of tunnel blockage and Reynolds number effects. Theoretical methods fail through inability to model separation effects, boundary layer displacement effects, or the interaction of the rotor wake with the fuselage pressure field. While it appears that the problems inherent in wind tunnel testing will remain with us, improvements in computer simulation may ultimately lead to analytical methods which will supplant the wind tunnel. In fact, a recent paper by Chapman, Mark and Pirtle (Reference 1) of the NASA-Ames Research Center, projects that this will occur within a decade if the current rate of advancement in computer technology continues. Although the complete solution of the Navier Stokes equations for flow around an arbitrary body remains beyond our present capability, much useful work has been done in the development of three-dimensional aerodynamic analysis tools. The ability to model separation would greatly enhance the usefulness of these methods.

Several approaches have been taken to model bluff body separation, i.e., by filling in the separated region with sources or a solid body fairing (Reference 2). These methods cannot predict the separation pressure levels directly, and consequently rely on some criterion to specify the pressure level. They do, however, generally improve the predicted pressure distributions upstream of separation. Improved performance prediction requires that the separated region pressure level be predicted as part of the overall analysis without recourse to empiricism. A separation model based on a vorticity shear layer approach which meets the above requirement has been developed and incorporated into a general

three-dimensional potential flow program. The separation model and the resulting analysis procedure are described in the following sections.

GENERAL APPROACH

An analysis procedure capable of predicting the three-dimensional aerodynamic characteristics of helicopter fuselage configurations having separated flow regions was the objective of the proposed study. In accomplishing this objective, two major tasks were completed:

(1) The modification of Computer program WBAERO in order to include viscous effects in the calculation of the potential flow. In this case, viscous effects include the displacement of external streamlines both by the upstream attached boundary layer and by the separated flow region. In many cases, a very thick but attached boundary layer will displace the external flow nearly as much as would a separation region.

(2) The development and verification of the vorticity separation model described in this report.

The general analysis procedure consists of a potential flow calculation, a boundary layer analysis, and a model of the separated flow. The analysis begins with the creation of planar surface panels from fuselage cross-section data input by the user. The inviscid flow field about this configuration is determined by the potential flow program. A series of streamlines are then calculated over the configuration surface, providing information required for the boundary layer methods. Laminar, transition, and turbulent boundary layer characteristics (including the separation point, if separation is present) are determined along each streamline, as are the source distributions representing the attached flow viscous effects. The separation points are used to map the separated flow region on the configuration geometry from which the vorticity shear layer leaves the surface. A new potential flow calculation is made with the inclusion of both the separation model and the boundary layer sources. The result is a predicted pressure field for the entire body in both attached and separated flow.

POTENTIAL FLOW METHOD

The potential flow on the body is computed using the WBAERO program described in Reference 3. The body surface is divided into a large number of planar panels, each of which contains a constant source distribution. In addition, an internal vortex lattice system may be located along the mean chord plane of lifting surfaces to provide circulation to the flow. A typical helicopter fuselage panel subdivision is shown in Figure 1.

GEOMETRY DEFINITION

The body is described by a series of cross-sections given at selected intervals along its length. The surface panels are located between adjacent sections, with the corner points being defined by the input cross-section coordinates. Although the standard WBAERO geometry input has been retained in the current program, it can easily be adapted to incorporate more sophisticated geometry inputs such as the Sikorsky Fuselage Geometry Definition Program, Reference 4.

INVISCID METHOD

Analytical expressions for the perturbation velocity field induced by a constant source distribution on an arbitrary quadrilateral panel are given by Hess and Smith (Reference 5). Similarly, the velocity field induced by the elements of a vortex lattice are given by Rubbert and Saaris (Reference 6). The perturbation velocities are used to calculate the coefficients of a system of linear equations relating the magnitude of the normal velocities at the panel control points to the unknown source and vortex strengths. The source and vortex strengths which satisfy the boundary condition of tangential flow at the control points for a given Mach number and angle of attack are determined by solving this system of equations by an iterative procedure. The pressure coefficients at panel control points are then calculated in terms of the perturbation velocity components, and the forces and moments acting on the configuration are obtained by numerical integration.

The perturbation velocity components induced by the sources and vortices are described in Reference 3, together with the formation and solution of the boundary condition equations, and the procedure used to calculate the pressure coefficients, forces, and moments on the configuration.

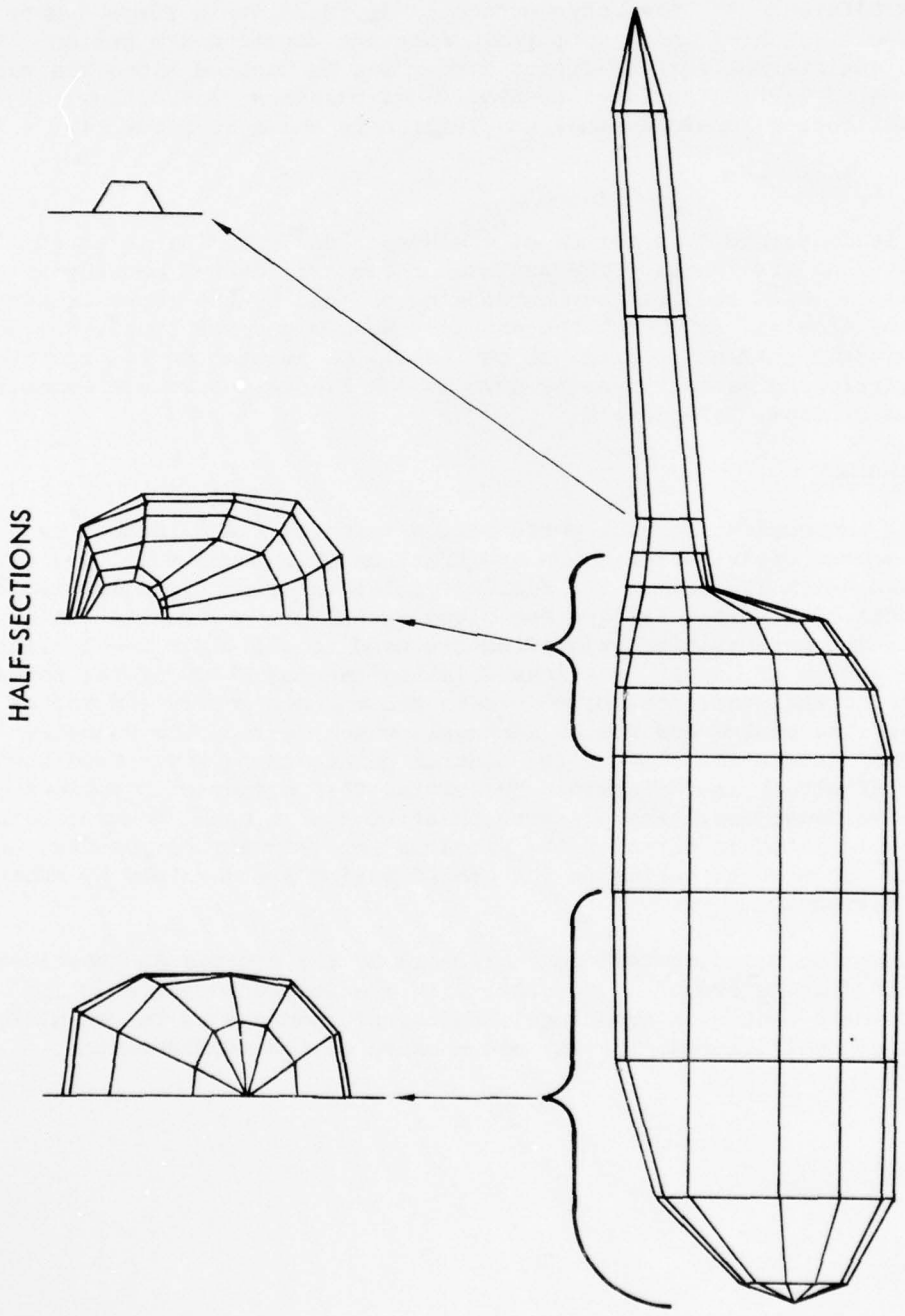

Figure 1. Paneling Arrangement on a Helicopter Fuselage.

STREAMLINE CALCULATION

The WBAERO program computes an approximate solution to the problem of three-dimensional potential flow over an arbitrary body. The body surface is represented by a set of plane quadrilaterals, and the three components of the velocity vector are computed at the panel centroids. The streamline program uses the velocity data at four neighboring panels to provide a linear approximation to the velocity anywhere on a given panel. A straight-line approximation to the actual streamline passing through a point on the panel is constructed, and continued over all panels upstream and downstream. This results in relatively smooth streamlines over the body, and allows the geodesic curvatures of the streamlines and equipotential lines to be computed. From this information, the metric or effective radius of the body along the streamline is obtained. The method used follows closely that described in Reference 7.

COMPUTATION OF THE PARTIAL DERIVATIVES

The quadrilateral under consideration, and its four neigbors, is shown on the following sketch. The quadrilateral coordinate system is identified by the letter Q, the upper neighbour by U, the lower by L, the upstream by T, and the downstream by R.

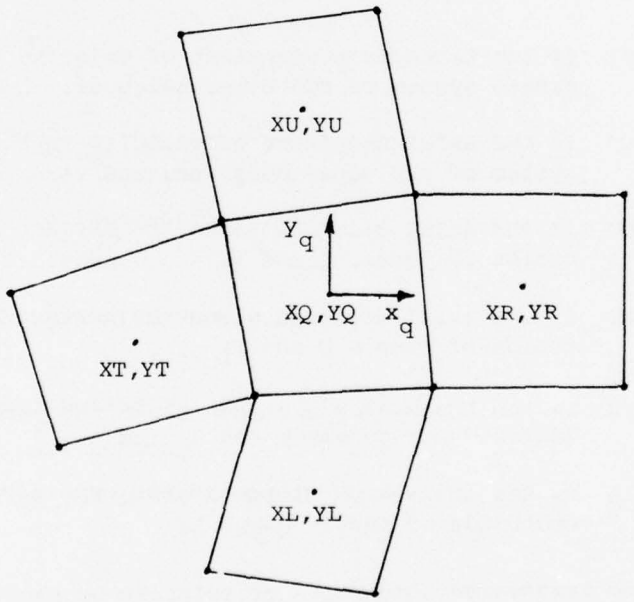

The neighboring panels are just assumed to be rotated about the common edges so that all panels lie in the same plane as the central quadrilateral. The program then computes the velocity and position vectors of the neighbors in terms of the central panel coordinate system. From this construction, the following partial derivatives are obtained.

$$U_1 = \frac{\partial U}{\partial x_q} = \frac{1}{2}\left(\frac{UR - UQ}{DXR} + \frac{UQ - UT}{DXT}\right) \tag{1}$$

$$U_2 = \frac{\partial U}{\partial y_q} = \frac{1}{2}\left(\frac{UU - UQ}{DYU} + \frac{UQ - UL}{DYL}\right) \tag{2}$$

$$V_1 = \frac{\partial V}{\partial x_q} = \frac{1}{2}\left(\frac{VR - VQ}{DXR} + \frac{VQ - VT}{DXT}\right) \tag{3}$$

$$V_2 = \frac{\partial V}{\partial y_q} = \frac{1}{2}\left(\frac{VU - VQ}{DYU} + \frac{VQ - VL}{DYL}\right) \tag{4}$$

where VU is the transverse component of velocity in the local coordinate system of the upper neighbor,

UU is the axial component of velocity in the local coordinate system of the upper neighbor, etc.,

DXR is the axial distance along the surface between the centroids of panels Q and R,

DXT is the axial distance along the surface bwtween the centroids of panels Q and T,

DYU is the transverse distance along the surface between the centroids of panels Q and U, and

DYL is the transverse distance along the surface between the centroids of panels Q and L.

The axial and transverse components of velocity on panel Q are then approximately:

$$U = U_q + U_1 x_q + U_2 y_q \qquad V = V_q + V_1 x_q + V_2 y_q \tag{5}$$

COMPUTATION OF POINTS ON A STREAMLINE

The streamline computation begins at a given point in a specified quadrilateral with the velocity vector, $\vec{V} = (U,V)$. A stream function is desired which will have a constant value of zero along the streamline. Since the divergence of $\vec{V}$ is not zero, an additional function, ρ, must be found such that the divergence of $\rho\vec{V}$ is zero. Then for a particle following a streamline

$$\frac{dy}{dx} = \frac{dy/dt}{dx/dt} = \frac{V}{U} = \frac{\rho V}{\rho U} \tag{6}$$

Thus a new vector field is constructed whose streamlines are identical to those of the velocity field, but whose divergence is zero. The function, ρ, is given by the series

$$\rho(x_q, y_q) = 1 - \frac{U_q (U_1 + V_2)}{U_q^2 + V_q^2} x_q - \frac{V_q (U_1 + V_2)}{U_q^2 + V_q^2} y_q + \ldots \tag{7}$$

The resulting stream function is

$$SF(x_q,y_q) = SF_0 - V_q x_q + U_q y_q - \left[V_1 - \frac{U_q V_q (U_1 + V_2)}{U_q^2 + V_q^2} \right] \frac{x_q^2}{2}$$

$$+ \left[U_2 - \frac{U_q V_q (U_1 + V_2)}{U_q^2 + V_q^2} \right] \frac{y_q^2}{2}$$

$$+ \left[U_1 - \frac{U_q^2 (U_1 + V_2)}{U_q^2 + V_q^2} \right] x_q y_q + \ldots \tag{8}$$

The constant value, SF_0, is chosen so that the stream function is zero at the specified point. Since the velocity is known only through the linear

terms, it is consistent to truncate the stream function after the quadratic terms.

Values of SF at the four corner points of the quadrilateral are now computed. By comparing the signs of SF at adjacent corners, the sides through which the streamline passes are determined. If the streamline passes through a side, the value of SF is computed at the midpoint of the side. From these three points, the intersection point is computed from a three-point interpolation formula.

The parameter, $t(0 \leq t \leq 1)$, is defined so that

$$x = x_1 + t(x_3 - x_1)$$

$$y = y_1 + t(y_3 - y_1) \tag{9}$$

Here, x,y is the intersection point,

x_1,y_1 is one corner point,

x_3,y_3 is the other corner point, and

x_2,y_2 is the middle point.

Then

$$0 = SF(x,y) = 2SF_1(t - \tfrac{1}{2})(t - 1) - 4SF_2 t(t - 1) + 2SF_3 t(t - \tfrac{1}{2}) \tag{10}$$

The root of this equation is chosen so that $0 \leq t \leq 1$. Note that if there had been two roots between 0 and 1, then SF would have the same sign at both corner points, and those intersection points would be ignored completely.

In general, two intersections will be found for the entire quadrilateral: one where the streamline enters, and one where it leaves. It is possible, however, for there to be four intersection points. The next point on the streamline is chosen from the intersection points as follows: a quantity, Q, is computed for each intersection point by taking the dot product of the vector from the starting point to the intersection point with the velocity vector at the centroid of the quadrilateral, and then multiplying it by the direction sign. (The direction sign is +1 if the streamline is being traced upstream.) The intersection point with the maximum

positive value of Q is chosen. However, if the largest Q is less than or equal to zero, none of the points is acceptable, and the program searches for another quadrilateral through which the streamline might pass.

Since each of the points representing a streamline is located at the boundary between two quadrilaterals, the values of the velocity and geodesic curvatures at each point can be computed separately for the two quadrilaterals. The average of the two values at a point is taken as the value at that point.

The streamline is first traced in the downstream direction, and then in the upstream direction. After the entire streamline has been obtained, the arc length along the streamline is computed so that it starts at zero at the upstream end. Points which are very close together are combined. Such points occur when the streamline cuts across a corner of a quadrilateral. If the distance between two points is less than one-eighth the distance between their neighbor in front and their neighbor in back, they are combined, and average values of their velocity, position, and curvatures are used for the new point.

COMPUTATION OF THE GEODESIC CURVATURES, (K_1 AND K_2), AND THE METRIC COEFFICIENT, H_2

The unit vector tangent to the streamline is

$$\vec{T} = \frac{\vec{i}U + \vec{j}V + \vec{k}W}{(U^2 + V^2 + W^2)^{\frac{1}{2}}} \tag{11}$$

where U, V, W are the components of the velocity vector, and

$\vec{i}$, $\vec{j}$, $\vec{k}$ are unit vectors in the three coordinate directions.

The curvature of the streamline is defined by

$$\vec{K} = d\vec{T}/d\ell \tag{12}$$

where ℓ is the arc length along the streamline. The geodesic curvature is the component of $\vec{K}$ on the body surface

$$K_g = \vec{K} \cdot (\vec{T} \times \vec{N}) \tag{13}$$

where $\vec{N}$ is the unit normal vector to the surface.

For a plane quadrilateral and with vectors written in the quadrilateral coordinate system, we have

$$\vec{T} = (\vec{i}U + \vec{j}V)/(U^2 + V^2)^{\frac{1}{2}} \tag{14}$$

$$\frac{d}{d\ell} = \left(U \frac{\partial}{\partial x} + V \frac{\partial}{\partial y}\right)/(U^2 + V^2)^{\frac{1}{2}} \tag{15}$$

$$\vec{K} = (\vec{i}V - \vec{j}U)\left[U(VU_x - UV_x) + V(VU_y - UV_y)\right]/(U^2 + V^2)^2 \tag{16}$$

where subscripts x and y denote partial differentiation

$$\vec{T} \times \vec{N} = (-\vec{i}V + \vec{j}U)/(U^2 + V^2)^{\frac{1}{2}}$$

Thus, K_2, the geodesic curvature for the streamline is obtained.

$$K_2 = \left[U(UV_x - VU_x) + V(UV_y - VU_y)\right]/(U^2 + V^2)^{\frac{3}{2}} \tag{17}$$

The geodesic curvature for the equipotential lines, K_1, is found by simply replacing U by V and V by -U in the equation for K_2

$$K_1 = \left[-V(VU_x - UV_x) + U(VU_y - UV_y)\right]/(U^2 + V^2)^{\frac{3}{2}} \tag{18}$$

The metric coefficient, H_2, is computed from the values of K_1. By definition,

$$K_1 = \frac{-1}{H_1 H_2} \frac{\partial H_2}{\partial \ell} \tag{19}$$

H_1 is defined to be unity along the streamline, so

$$H_2 K_1 = -\frac{\partial H_2}{\partial \ell} \tag{20}$$

This equation is approximated by

$$H_2(\ell + \Delta\ell) - H_2(\ell) = -\frac{\Delta\ell}{2}\left[H_2(\ell)\, K_1(\ell) + H_2(\ell + \Delta\ell)\, K_1(\ell + \Delta\ell)\right]$$

or

$$H_2(\ell + \Delta\ell) = H_2(\ell)\left[\frac{2 - \Delta\ell\, K_1(\ell)}{2 + \Delta\ell\, K_1(\ell + \Delta\ell)}\right] \tag{21}$$

where $\Delta\ell$ is the chord length of the segment of the streamline passing through the quadrilateral.

Note that H_2 is determined only to within a multiplication constant. This constant was arbitrarily chosen so that H_2 is unity at the specified starting point for the streamline. Thus, for an axisymmetric body, H_2 will be proportional to the radius, but it will not, in general, equal the radius.

BOUNDARY LAYER METHODS

The boundary layer development on an arbitrarily shaped three-dimensional lifting configuration can be very complex. A thorough and exact calculation of this development is properly the domain of the time-dependent solution to the general Navier Stokes equations. Unfortunately, the computer does not yet exist which is capable of handling such a problem, and even if one did, the cost in computer time would be astronomical. Less difficult or costly are the three-dimensional boundary layer programs now in existence (References 8, 9 and 10). These are, however, all finite difference methods which are complex, difficult to use (see Nash, Reference 8), and generally very configuration dependent. The amount of computer time required for each calculation still prohibits their use in an analysis procedure of the type reported herein. Having made the above evaluation, one must conclude that if the objective is a viscosity-dependent calculation procedure of practical use to the aerodynamicist for drag analysis and, possibly, for preliminary design, the method must be relatively simple to use and economic of computer time. This can only be achieved if integral boundary layer methods are used. In two dimensions, integral methods are typically about 100 times faster than finite difference methods. When compared with three-dimensional finite difference methods, the time disparity becomes considerably greater.

The use of integral methods along external streamlines taking into account streamline convergence or divergence has proven to be a valid and reliable approach. They can, however, be expected to break down in regions of large streamline convergence or divergence (regions of large crossflow). As shown in the photographs of Reference 2, this occurs usually in the region of separation where none of the boundary layer methods (including three-dimensional) can be expected to be valid. It is anticipated, therefore, that integral methods will suffice for most applications of interest to the aerodynamicist for drag prediction or preliminary design.

In those cases of special interest to the aerodynamicist, such as the effect of area suction for boundary layer control or of roughness (rivets, etc.) on drag, alternate boundary layer calculation modules are available. These methods are called as needed into the overall calculation procedure A brief description of all of the boundary layer methods is given in the following paragraphs.

LAMINAR METHOD

The integral method is an adaption by Curle (Reference 11) of a method developed by Thwaites (Reference 12). In Thwaites' method, the momentum integral equation

$$d\theta/dx = C_f/2 - (H + 2)(\theta/U)(dU/dx) - (\theta/r)(dr/dx) \tag{22}$$

is written in the form

$$(d/dx)(K/U) = L/U - (K/r)(dr/dx)/(dU/dx) \tag{23}$$

where

$$\begin{aligned} K &= \theta^2/\nu(dU/dx) \\ L &= \{\ell - K(H + 2)\} \\ \ell &= (\theta/U)(\partial U/\partial y)_{y=0} \end{aligned} \tag{24}$$

$\frac{1}{r}\frac{dr}{dx}$ = a measure of the streamline divergence or convergence

In Thwaites' method, the divergence term was not considered, although the method was later extended to include this term by Rott and Crabtree (Reference 13).

Thwaites used exact solutions to a variety of laminar flows to determine the relationship between L and K,

$$L = 0.45 - 6K \tag{25}$$

Curle has pointed out that Equation (25) is not adequate in flows approaching separation, and he has suggested an extension or correction giving

$$L = 0.45 - 6K + g(K,\mu) \tag{26}$$

The parameter, μ, is a function of both the pressure gradient and the curvature or second derivative of velocity.

$$\mu = K^2 U(d^2U/dx^2)/(dU/dx)^2 \tag{27}$$

Curle rewrote Equation (26) in the form

$$L = F_o(K) - \mu G_o(K) \tag{28}$$

where F_o and G_o are universal functions determined from a series of exact solutions to laminar flows in the same way as they are in Equation (25). After substitution of Equation (26) into Equation (23), and with subsequent integration, the result can be rearranged in the form

$$\theta^2 = 0.45\nu/(U^6 r^2) \int_o^x r^2(1 + 2.22g)U^5 dx \tag{29}$$

This equation is conveniently solved by iteration, g initially equal to zero. With values of K and μ determined in the first iteration, a second iteration is carried out using Equation (28). At each step in the calculation, the local skin friction coefficient, C_f, and the shape factor, H, can be calculated using Equation (24). The local skin friction coefficient has been defined as

$$C_f = (\mu/\rho\theta U)\ell \tag{30}$$

where ℓ in Equation (24) is determined in a similar manner to L from a series of known solutions to give

$$\ell^2 = F_1(K) - G_1(K) \tag{31}$$

The functions F_o, F_1, G_o and G_1 are tabulated in the computer program. Calculations begin at the stagnation point, with the initial momentum thickness, θ, given as a function of K. For bluff bodies, K takes an initial value ($K_o = 0.0604$) at the stagnation point, from which the initial momentum thickness, θ_o, is

$$\theta_o = (.0604/dU/dx)^{1/2} \tag{32}$$

The calculation proceeds either to laminar separation or to the end of the airfoil, whichever occurs first. The calculated boundary layer development is then interrogated to determine if transition, laminar separation

or forced transition (boundary layer tripping) has taken place. If any of these phenomena have occurred, the downstream flow is assumed to be turbulent.

Boundary Layer Transition and Laminar Separation

Boundary layer transition is a very complex phenomenon, and to date no completely reliable general theoretical method has been developed for its prediction. Reynolds number is a controlling parameter, but it has been shown that the Reynolds number at transition can be increased a considerable amount by careful elimination of disturbances. At very low Reynolds numbers, laminar boundary layers are stable to small disturbances. However, at higher Reynolds numbers, the boundary layer is unstable, and small disturbances can be amplified. Amplification of these disturbances causes the flow to become turbulent. The point at which flow breakdown occurs depends on the strength and dominant frequency of the initial disturbance. Disturbances may be due to freestream turbulence, surface roughness, noise or vibration of the surface. As there is no detailed analysis of the transition process, transition prediction is accomplished by means of empirical correlations. Granville (Reference 14) has developed a procedure based on the determination of the neutral stability point and the transition point. The neutral stability point is defined as that point downstream from which small disturbances are amplified within the boundary layer. It is this amplification of small disturbances that ultimately leads to transition. The neutral stability point is reached when the Reynolds number, based on the local momentum thickness and local flow properties, attains some critical value, $R_{\theta_{ins}}$. Schlichting and Ulrich (Reference 15) have shown that $R_{\theta_{ins}}$ can be correlated with the local pressure gradient parameter, $K = (\theta^2/\nu)(dU/ds)$. Correlations by Smith (Reference 16) and others have been reduced to analytical form as follows.

Instability Curves

$$K = -0.4709 + 0.11066 \ln R_\theta - 0.0058591 \ln^2 R_\theta \qquad (33)$$

$$\text{for } 0 < R_{\theta_{ins}} \leq 650$$

and

$$K = 0.69412 - 0.23992 \ln R_\theta + 0.0205 \ln^2 R_\theta \qquad (34)$$

$$\text{for } 650 < R_{\theta_{ins}} \leq 10{,}000.$$

If for a given R_θ the pressure gradient parameter, K, as calculated by Equation (33) or (34), is greater than that determined by the boundary layer developemnt, the flow has passed from a stable to an unstable region. Once the flow passes into the unstable region, the transition process begins; and Granville has been able to show that a correlation similar to the instability process can be used to determine the transition point. He formed an average pressure gradient parameter, K, defined as

$$\bar{K} = \frac{\int_{s_{ins}}^{s_{trans}} K \, ds}{s_{trans} - s_{ins}} \tag{35}$$

which correlated reasonably well with the momentum thickness Reynolds number at transition $R_{\theta_{trans}}$. This correlation is presented in analytical form as follows.

Transition Curves

$$\bar{K} = -0.0925 + 7.0 \times 10^{-5} R_\theta \tag{36}$$

$$\text{for } 0 < R_{\theta_{trans}} \leq 750,$$

$$\bar{K} = -0.12571 + 1.14286 \times 10^{-4} R_\theta \tag{37}$$

$$\text{for } 750 < R_{\theta_{trans}} \leq 1{,}100$$

and

$$\bar{K} = 1.59381 - 0.45543 \ln R_\theta + 0.032534 \ln^2 R_\theta \tag{38}$$

$$\text{for } 1{,}100 < R_{\theta_{trans}} \leq 3{,}000.$$

When the $\bar{K}$ calculated by one of the above expressions for a given R_θ is greater than the value determined from the boundary layer development, transition is predicted.

With transition predicted, initial values of the momentum thickness, θ, and the shape factor, H, are required to start the turbulent boundary

layer calculation. Because the boundary layer growth is continuous, the momentum thickness at transition is used as the initial turbulent momentum thickness. Since the shape factor varies from values greater than 2.0 to less than 1.5 through the transition region, an empirical expression is used to determine the initial turbulent shape factor. The empirical relation between H and $R_{\theta_{trans}}$ was determined from data obtained by Coles (Reference 17):

$$H_t = \frac{1.4754}{\text{Log}_{10} R_{\theta_{trans}}} + 0.9698 \tag{39}$$

In many cases, the pressure gradient is of sufficient strength to separate the laminar boundary layer prior to transition. Except in extreme cases, the boundary layer will then reattach, usually as a turbulent boundary layer. Only recently have researchers been able to analyze this phenomenon (Reference 18), and as yet the procedure is extremely complicated and cumbersome; consequently, empirical relationships are still required. From the measurements of Gaster (Reference 19) and others, a correlation is formed which is capable of predicting both the occurrence of a separation and later the reattachment as a turbulent boundary layer or the catastrophic separation. The correlation is of the form

$$K = 0.27 - 0.0007575\, R_\theta - 0.000001157\, R_\theta^2 \tag{40}$$

for $R_\theta > 125$

and

$$K = -.09 \tag{41}$$

for $R_\theta < 125$.

If K becomes less than -0.09, separation occurs, and if R_θ is less than 125, the boundary layer is not able to reattach. However if R_θ is greater than 125, the value of K determined by the boundary layer development must be less than that calculated by Equation (40) before separation without reattachment is predicted. If reattachment is predicted, the turbulent boundary layer calculation is initiated using the momentum thickness calculated at the separation point.

TURBULENT METHOD

Methods for the calculation of turbulent boundary layers in two dimensions have been developed by many investigators. These methods were reviewed at a conference held in 1968 at Stanford University (Reference 20). One of the methods, an integral method by Nash and Hicks (Reference 21), compared very favorably with the more complex finite difference methods. Now, several years later, the method remains an excellent approach for application to the current problem, both in terms of accuracy and speed.

The Nash-Hicks method is based on momentum and moment of momentum equations coupled with a skin friction law derived from Coles' velocity profile family (Reference 22). An additional equation is obtained by relating the shear stress integral to its equilibrium value using a simple first-order differential equation. The equations have been derived in References 23 and 24, and are repeated herein for completeness.

A family of integral equations can be derived taking higher moments of the equation of motion. The resulting equations can be expressed as

$$\int_0^\delta \left\{ u \frac{\partial u}{\partial x} - \frac{1}{r} \frac{\partial u}{\partial y} \int_0^\delta \frac{\partial (ur)}{\partial x} \, dy \right\} y^\alpha dy = \frac{U\delta^{\alpha+1}}{\alpha + 1} \frac{dU}{dx} + \frac{1}{\rho} \int_0^\delta y^\alpha \frac{\partial \tau}{\partial y} \, dy \qquad (42)$$

where $\alpha = 0$ gives the momentum integral equation, and

$\alpha = 1$ gives the moment of momentum integral equation

The velocity distribution across the boundary layer can be represented by Coles' velocity profile family, given by

$$u = \frac{u_\tau}{\kappa} \left\{ \ln \left(y \frac{u_\tau}{\nu} \right) + C \right\} + \frac{u_\beta}{2} \left\{ 1 - \cos \frac{(\pi y)}{\delta} \right\} \qquad (43)$$

where u_τ = friction velocity $(\tau_w/\rho)^{\frac{1}{2}}$

u_β = free parameter having units of velocity,

δ = boundary layer thickness,

κ = .41, and

$$C = 2.05.$$

Substitution of this equation into Equation (42) results in two equations of the form:

$$A \frac{du_\tau}{dx} + B \frac{du_\beta}{dx} + \frac{C}{\delta} \frac{d\delta}{dx} + \Phi = D \frac{dU}{dx} - \frac{E}{r} \frac{dr}{dx} \tag{44}$$

A third equation of the same form is obtained by evaluating Equation (43) at $y = \delta$ followed by the differential with respect to x. The parameter, Φ, is represented by the following relations:

$$\begin{aligned} &\text{(i)} \quad \alpha = 0 && \Phi = \frac{-1}{\delta} u_\tau^2 \\ &\text{(ii)} \quad \alpha = 1 && \Phi = \frac{-1}{\delta^2} \int_0^\delta \frac{\tau}{\rho} \, dy \\ &\text{(iii)} \quad \alpha = \infty && \Phi = 0 \end{aligned} \tag{45}$$

The shear stress integral, $\int_0^\delta \frac{\tau}{\rho} \, dy$, appearing in Equation (45) was evaluated by Nash and Hicks using an equation of the form

$$\frac{d C_\tau}{dx} = \frac{.15}{\delta} (C_{\tau_{eq}} - C_\tau) \tag{46}$$

where $$C_\tau = \frac{1}{1/2\rho U^2 \delta} \int_0^\delta \tau dy$$

The equilibrium value of C_τ, $(C_{\tau_{eq}})$ was determined by Nash and Macdonald, Reference 23, from measured shear stress distributions giving

$$C_{\tau_{eq}} = .025 \left(1 - \frac{1}{H}\right)^2 \tag{47}$$

where H is the local shape factor. Equation (47) can be expressed in terms of the parameters u_τ, u_β and U by evaluation of the integral relations used to define H; that is,

$$H = \frac{\delta^*}{\theta} = \frac{\int_0^\delta (1 - \frac{u}{U})\, dy}{\int_0^\delta \frac{u}{U}(1 - \frac{u}{U})\, dy} \tag{48}$$

with the aid of Equation (43). The equations for the four unknowns, u_τ, u_β, δ and C_τ, can be integrated once the pressure distribution, U(x), and the streamline divergence, 1/r(dr/dx), are prescribed. Initial conditions are obtained from the transition analysis. In this case, initial values of the momentum thickness, θ, and the shape factor, H, are known. Initial values of u_τ, u_β and δ can be determined from the known θ and H using Equation (43). The starting value for C_τ is obtained by making the assumption that in the region of transition, $C_\tau \simeq C_{\tau_{eq}}$.

The accuracy of the calculation method is demonstrated in Figure 2. This figure shows a comparison between measured and calculated boundary layer developments along a streamline on the U.S. Airship Akron. A further comparison is shown in Figure 3 for the case of a boundary layer in a strong, adverse pressure gradient approaching separation. Particular reference should be made to the good agreement between calculated and measured skin friction coefficients.

ROUGHNESS AND AREA SUCTION

The contribution of such roughness elements as rivets to the overall drag of a helicopter fuselage is small when compared to drag due to separation. However, as separation-free designs gain in interest, attention to such items as roughness drag becomes important. The calculation method of References 25 and 26 is used when rough surfaces are present to determine the effect of roughness on the downstream boundary layer development and on skin friction drag. This method, which is an extension of Head's original entrainment method, is based on the momentum integral equation (Equation (22)) and the entrainment equation (Reference 27).

$$d(\delta - \delta^*)dx = F(H_1) - (\delta - \delta^*)\left[du/dx/u + dr/dx/r \right] \tag{49}$$

The parameter, $H_1 = (\delta - \delta^*)/\theta$, is related to the conventional form parameter, H, by

$$H_1 = G(H) \tag{50}$$

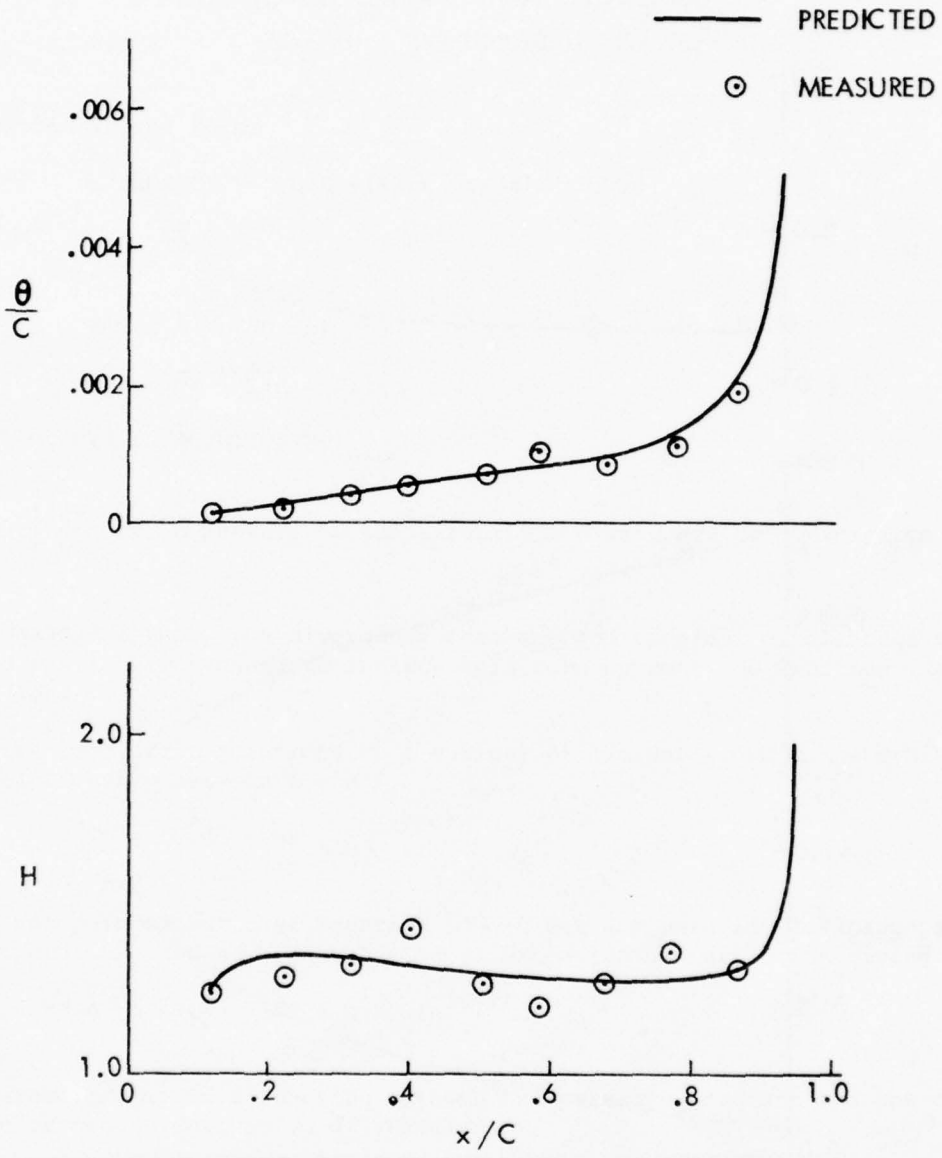

Figure 2. Comparison of Measured and Predicted Boundary Layer Developments on U. S. Airship Akron.

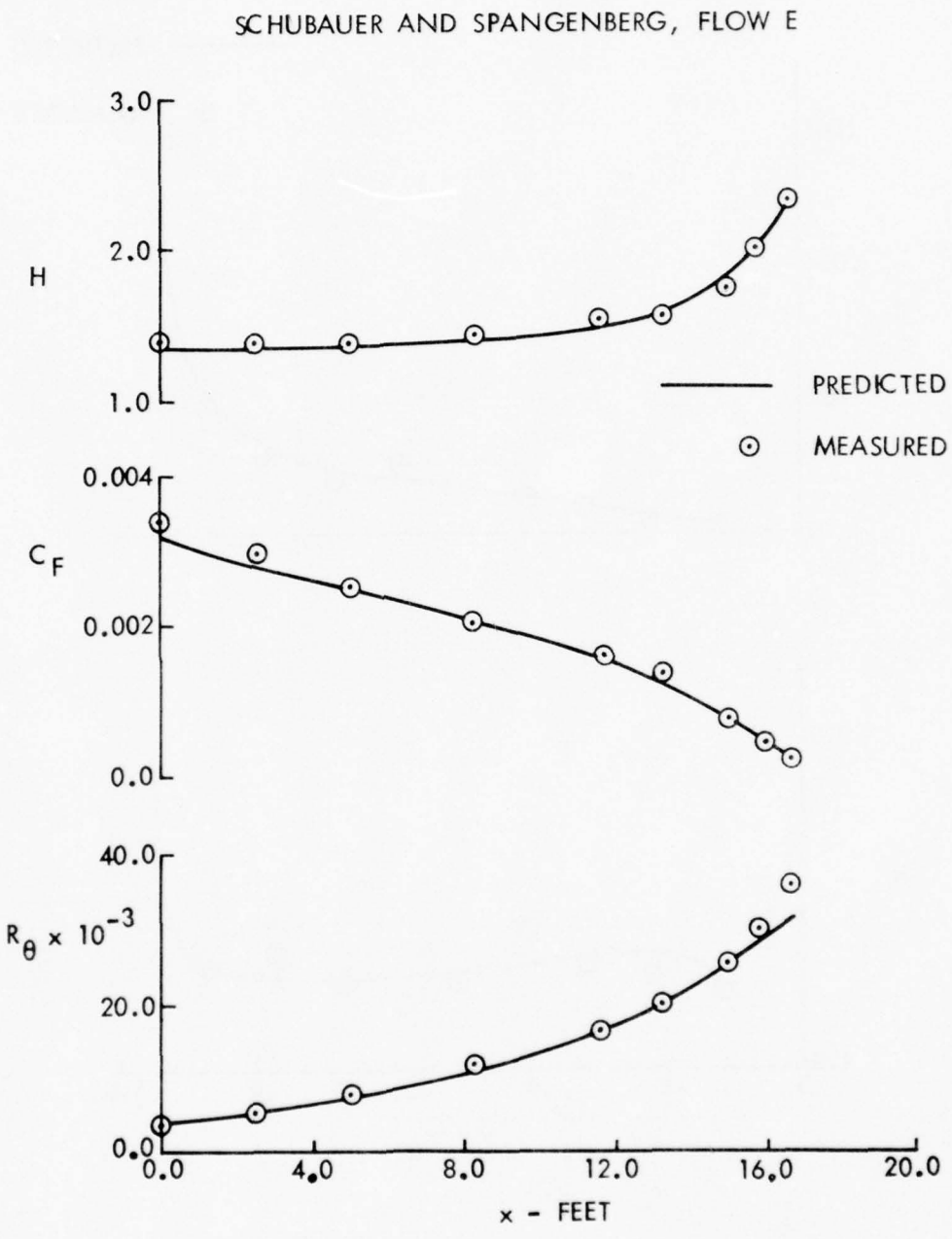

Figure 3. Comparison of Measured and Predicted Boundary Layer Developments.

The entrainment functions, $F(H_1)$ and $G(H)$, have been defined numerically as

$$F(H_1) = \exp\left[-3.512 - 0.617\ \ell n\ (H_1 - 3.)\right] \tag{51}$$

and

$$G(H) = 3.3 + \exp\left[0.4667 - 2.722\ \ell n\ (H - 0.6798)\right] \tag{52}$$

for $H \leq 1.6$ or

$$G(H) = 3.3 + \exp\left[0.4383 - 3.064\ \ell n\ (H - 0.6798)\right] \tag{53}$$

for $H > 1.6$.

The effect of roughness enters through the skin friction law which can be expressed as

$$(2/c_f)^{\frac{1}{2}} = 5.6 \log_{10} U\delta^*/\nu + 4.8 - \Delta U_1/U_\tau + \Delta U_2/U_\tau \tag{54}$$

where $\Delta U_1/U_\tau$ represents the modifications of the velocity profile near the wall in the vicinity of roughness elements. $\Delta U_1/U_\tau$ has been shown to be a function of the roughness spacing (density) as well as the roughness height. In the density range, $1 \leq \lambda \leq 5$, where λ is the ratio of total surface area to roughness area, the variation of $\Delta U_1/U_\tau$ with roughness can be specified by

$$\Delta U_1/U_\tau = 5.6 \log_{10} U_\tau k/\nu + 17.35\ (1.625 \log_{10} \lambda - 1) \tag{55}$$

and in the range $\lambda > 5$ by

$$\Delta U_1/U_\tau = 5.6 \log_{10} U_\tau k/\nu - 5.95\ (1.103 \log_{10} \lambda - 1) \tag{56}$$

The function $\Delta U_2/U_\tau$ represents the effect of pressure gradient on the skin friction, both on smooth or rough surfaces, and is defined as follows.

$$\Delta U_2/U_\tau = 1.253\ (G - 6.7) \tag{57}$$

for $G \geq 6.7$ (adverse pressure gradient), and

$$\Delta U_2/U_\tau = 0.404\ (G - 6.7) \tag{58}$$

for $G < 6.7$ (favorable pressure gradient).

The parameter, G, is Clauser's pressure gradient parameter given by

$$G = (2/C_f)^{\frac{1}{2}} (H - 1)/H \tag{59}$$

The entrainment equations, Equations (49) and (50), may be integrated simultaneously with the momentum integral equation, with the skin friction coefficient being determined at each step in the calculation from Equation (54) to give the turbulent boundary layer development. The calculation is begun at the transition point with initial values of the shape factor, H, and the momentum thickness, θ, determined from the laminar and transition calculations. The roughness height distribution, k/c, the roughness density, λ, the pressure distribution, and the stream divergence distribution are all assumed known.

The effect of area suction on the development of the turbulent boundary layer is readily accounted for by adding the ratio of suction velocity to free-stream velocity (V_w/U) to the right-hand side of both the momentum integral and entrainment equations. A different skin friction law must, however, be used to determine the effect of suction on the local skin friction coefficient. This is provided by the work of Thompson, whereby a skin friction law of the form

$$C_f = f(H, R_\theta, V_w/U) \tag{60}$$

is derived. For a given suction distribution, the boundary layer development is calculated using Equation (22) in conjunction with Equations (49) and (50).

VISCOUS/INVISCID INTERACTION

The effect of boundary layer displacement on the potential flow is simulated by distributing sources of known strength on the panels used to describe the fuselage geometry. The strengths of these sources are determined directly from the boundary layer solutions as $q_i = \frac{d}{ds} (U_i \delta_i^*)$, where U_i is the streamwise potential flow velocity at the edge of the boundary layer, and δ_i^* is the streamwise displacement thickness. The addition of this source distribution modifies the normal velocity at the control point of panel i. Consequently, the boundary condition (Reference 3) is modified as follows

$$V_{ni} = R_i + q_i + \sum_{j=1}^{N} a_{ij} \sigma_j \tag{61}$$

Since q_i is known for each iteration, only the right-hand side of Equation (61) is altered, giving (in matrix notation)

$$\left[A_{ij} \right] \sigma_j = -R_i - q_i \tag{62}$$

Because the original geometry is not modified by the use of distributed sources, the aerodynamic influence coefficient matrix need not be recalculated. Subsequent iterations between the potential flow and boundary layer calculations result in convergent solutions. The alternative procedure (modifying the geometry directly by addition of the displacement thickness) while quite widely used in two dimensions, becomes untenable in three dimensions. Primarily, this is a result of having to calculate and invert a new aerodynamic influence coefficient matrix at each iteration due to the change in geometry. Without considering the additional cost of smoothing the geometry and redefining the panels at each iteration, the additional cost of calculating and inverting the influence coefficient matrix at each iteration would be prohibitive.

CALCULATION PROCEDURE

The computer program is made up of a series of overlays, as shown in Figure 4. The executive program, DRAG, controls the overall analysis by calling in turn the overlays containing the potential flow and boundary layer calculation methods. The calculation sequence is outlined as follows.

1. The input geometry, as represented by a series of planar panels, is lofted in Program WBPAN. An alternate slot is provided under the heading Program GEOMETRY for such time as an improved geometry program becomes available.

2. The potential flow pressure field is computed for the fuselage configuration in Program WBAERO.

3. Up to six streamlines are calculated in Program STREEM. These streamlines pass through the midpoints of prescribed panels.

4. The laminar and turbulent boundary layer developemnts are determined for each streamline using pressure, arc length, and streamline divergence distributions calculated in Program STREEM. Transition or laminar separation and turbulent separation are predicted, if present. Program INTGRAL is used for the integral boundary layer analysis; and currently, three options are available for the turbulent boundary layer analysis: for boundary layers on smooth surfaces, rough surfaces, or with area suction

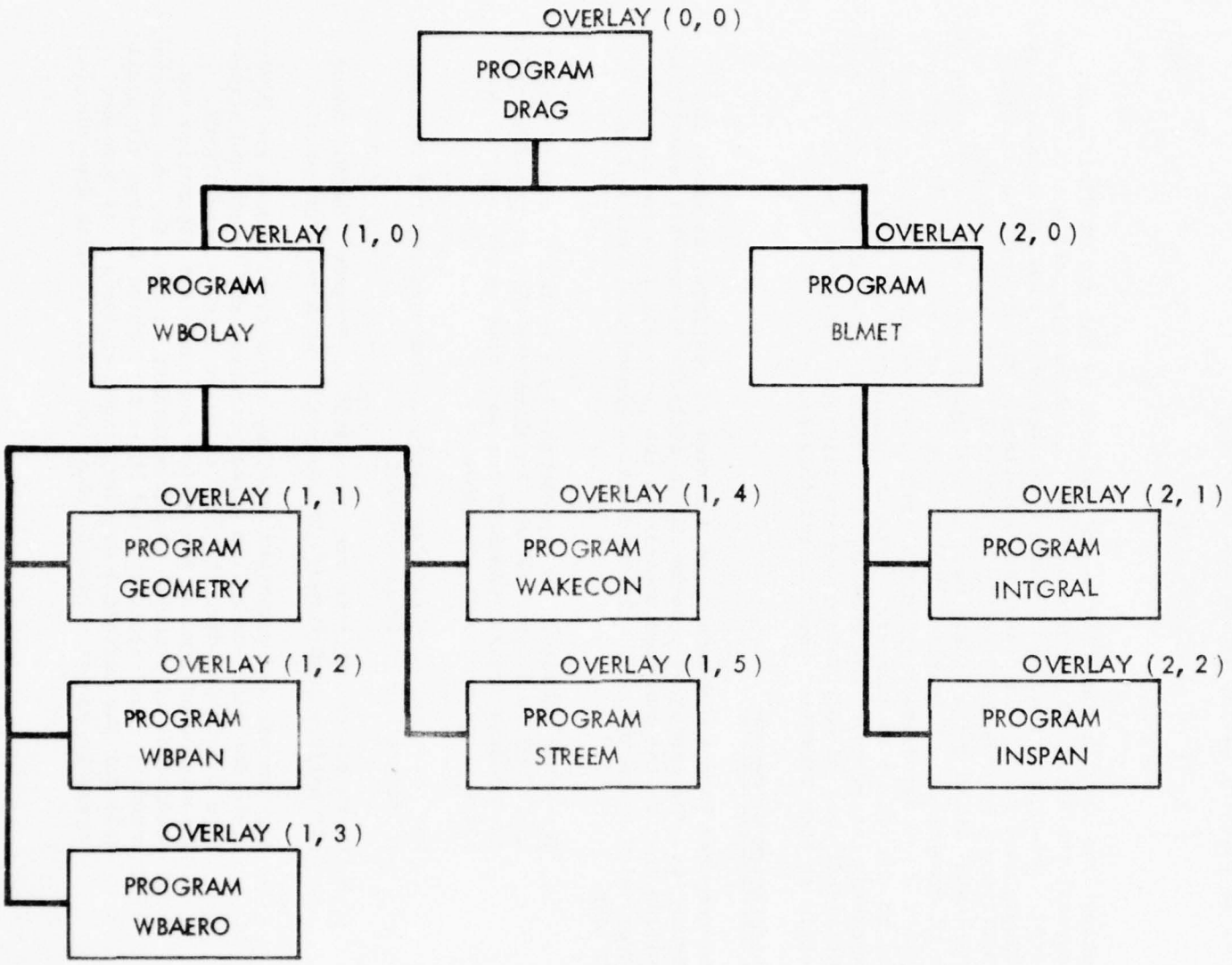

Figure 4. Overlay Structure of the Calculation Procedure.

boundary layer control. A slot is provided for Program INSPAN, the finite difference method for tangential blowing boundary layer control. This program will be made available at a later date.

5. Source distributions representing the boundary layer displacement effect are determined for each streamline.

6. The separated flow region is determined in Program WAKECON. The separation model is prescribed, and a new potential flow solution (with the boundary layer source distribiton included) is obtained. Base pressures are determined, and the drag is calculated.

Steps 3 through 6 are repeated a second time if required. The calculation procedure is illustrated in Figure 5.

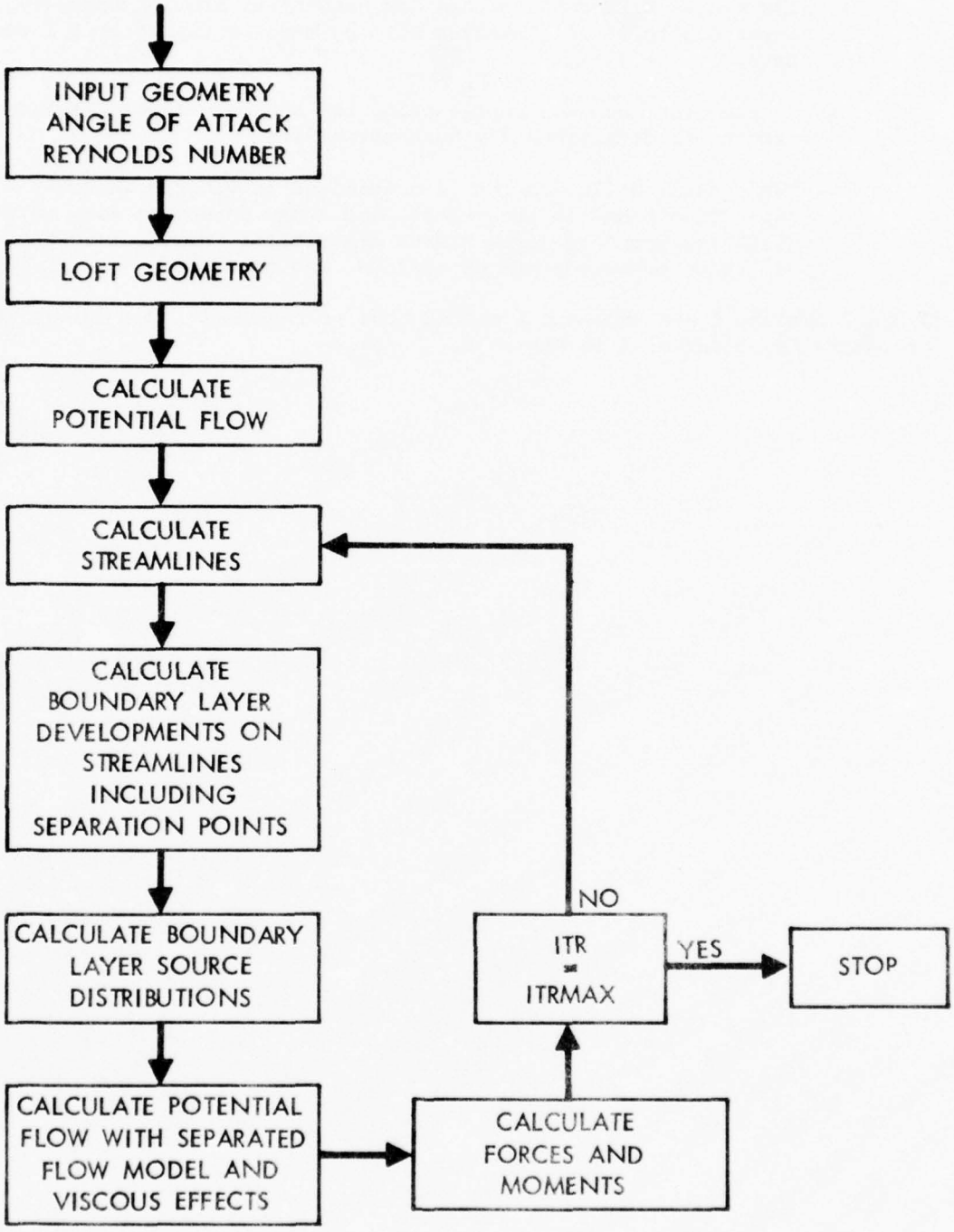

Figure 5. Flow Diagram of the Calculation Procedure.

DEVELOPMENT OF THE SEPARATED-FLOW MODEL

DESCRIPTION OF THE REAL FLOW

Four regions are identifiable in the flow field around a body with separation (Figure 6).

Region 1 - The Potential Flow region

The region exterior to the boundary layer and separated wake is almost precisely irrotational since the shear is so low that viscous stresses impart a negligible rotation to the fluid (originally irrotational upstream of the body). All of the regions are almost solenoidal* since we are assuming the Mach number to be low enough to make compressibility negligible. Thus the region is very nearly a potential flow (i.e., irrotational and solenoidal).

Region 2 - The Boundary Layer

The thin flow region next to the airfoil surface has high shear, and hence, viscous stresses which create significant vorticity.

Region 3 - The Free Shear Layer

The thin flow region fed by the separating boundary layer has rotation but only moderate shear. The vorticity transport is predominantly by convection, although diffusion is not insignificant.

Region 4 - The Wake

The wake between the two shed boundary layers is a region with low vorticity and insignificant viscous stresses. This region has a lower total head than that of the onset flow.

TWO-DIMENSIONAL METHOD

A simple theoretical model of the real flow is shown in Figure 7. This model was developed in two-dimensional flow before proceeding to the three-dimensional case. In order to be compatible with the WBAERO method, the body is represented by a number of constant-source panels, and the free shear layers by uniform vorticity panels aligned in the free-stream direction. (Later developments should consider calculating the vortex panel orientation.) The vorticity panels must be attached to the body at the source panel edges nearest to the separation point. This restriction is necessary to avoid numerical problems associated with the abrupt change

*Solenoidal means vanishing divergence, the mass conservation requirement for a steady, incompressible flow.

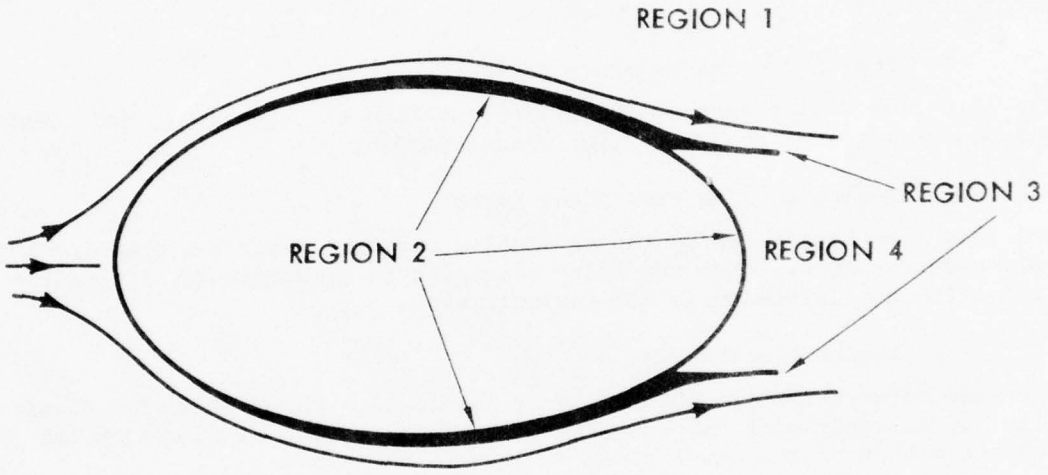

REGION 1 - POTENTIAL FLOW REGION

REGION 2 - BOUNDARY LAYER

REGION 3 - FREE SHEAR LAYER

REGION 4 - WAKE

Figure 6. Regions in the Real Flow.

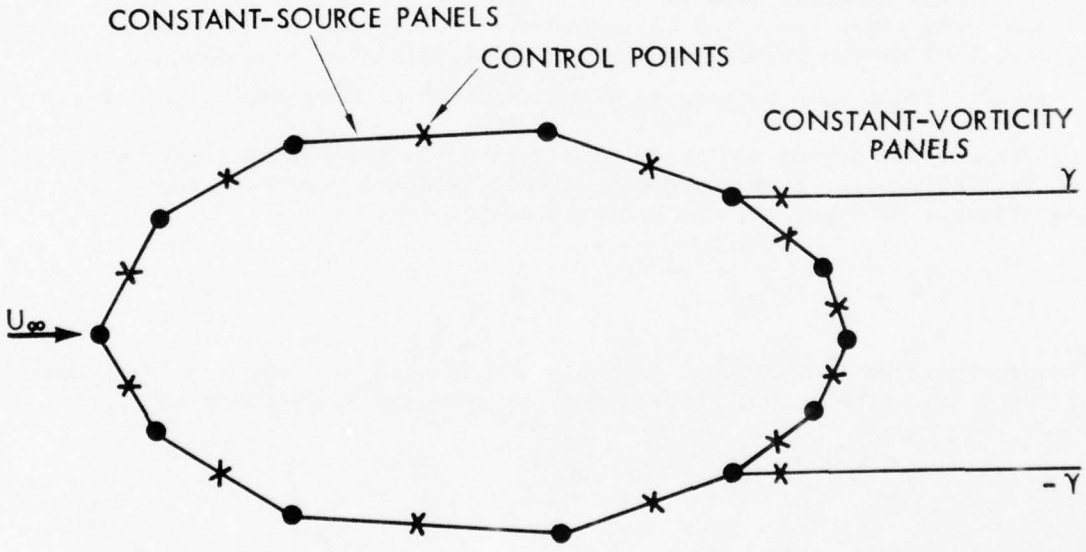

Figure 7. Theoretical Model Using Source and Vortex Panels.

from source to vortex panels.

The boundary condition of zero normal velocity is specified at a control point in the middle of each surface source panel. In addition, the boundary condition of the streamwise flow is specified on the vortex panels at points directly above the source panel control point downstream of the separation point (Figure 7). Considering a symmetrical case, we can use, say, N source panels and one vortex panel on half of the body. This gives N + 1 control point equations in N unknown source panel densities, and one vorticity value. The equations are of the form

$$A_{jk}\,\sigma_k + B_j\gamma = C_j \qquad : \quad k = 1, 2, \ldots, N \qquad (63)$$
$$j = 1, 2, \ldots, N + 1$$

where A_{jk} is the influence coefficient for the normal component of velocity induced at the j^{th} panel's control point by the k^{th} source panel; B_j is the influence coefficient for the normal component of velocity induced at the j^{th} panel's control point by the vortex panel; and C_j is the normal component of the onset flow at the j^{th} panel's control point. Later, when the boundary layer procedure is included to calculate the separation point, C_j will include the boundary layer source distribution representing displacement effect (see Section on Viscous/Potential Flow Interaction).

Solution of the system of linear equations gives the source distribution and vorticity value from which the surface pressures are evaluated. In the attached flow region, the pressure coefficient is

$$C_p = 1 - \left(\frac{V}{U_\infty}\right)^2$$

In the separated flow region, there is a reduction in total head from that of the free stream. Here, therefore, the pressure coefficient is

$$C_p = 1 - \left(\frac{V}{U_\infty}\right)^2 - \frac{\Delta H}{\frac{1}{2}\rho U_\infty^{\,2}}$$

The reduction in total head, ΔH, can be evaluated by considering the conditions on the free shear layer. On the outer edge of the layer

$$C_{p_o} = 1 - \left(\frac{V_o}{U_\infty}\right)^2$$

and on the inner edge

$$C_{p_i} = 1 - \left(\frac{V_i}{U_\infty}\right)^2 - \frac{\Delta H}{\frac{1}{2}\rho U_\infty^2}$$

and since the layer cannot support a pressure difference across it, then $C_{p_o} = C_{p_i}$, and

$$\frac{\Delta H}{\frac{1}{2}\rho U_\infty^2} = \left(\frac{V_o}{U_\infty}\right)^2 - \left(\frac{V_i}{U_\infty}\right)^2$$

or $$\Delta H = \tfrac{1}{2}\rho (V_o - V_i)(V_o + V_i)$$

But $(V_o - V_i)$ is the vorticity value in the layer, i.e., γ, which is part of the solution, and $\frac{1}{2}(V_o - V_i)$ is the mean velocity, V_M, say, in the layer. Therefore,

$$\Delta H = \rho V_M \gamma$$

and the pressures in the separated region are

$$C_p = 1 - \left(\frac{V}{U_\infty}\right)^2 - \frac{2V_M\gamma}{U_\infty^2}$$

The mean velocity, V_M, in the shear layer is readily calculated once the singularity strengths are known.

Initial computations based on a circular cylinder showed that the peak suction upstream of separation was underestimated when using a long wake panel. It was found that a shorter wake length gave good agreement with experimental pressures over the whole cylinder. This sensitivity of the solution to the assumed wake length is illustrated in Figure 8 for a circular cylinder with separation at 105^0. The wake length which gives good agreement with the experimental base and peak suction pressures (from Reference 28) in this case is about 20% larger than the cylinder diameter.

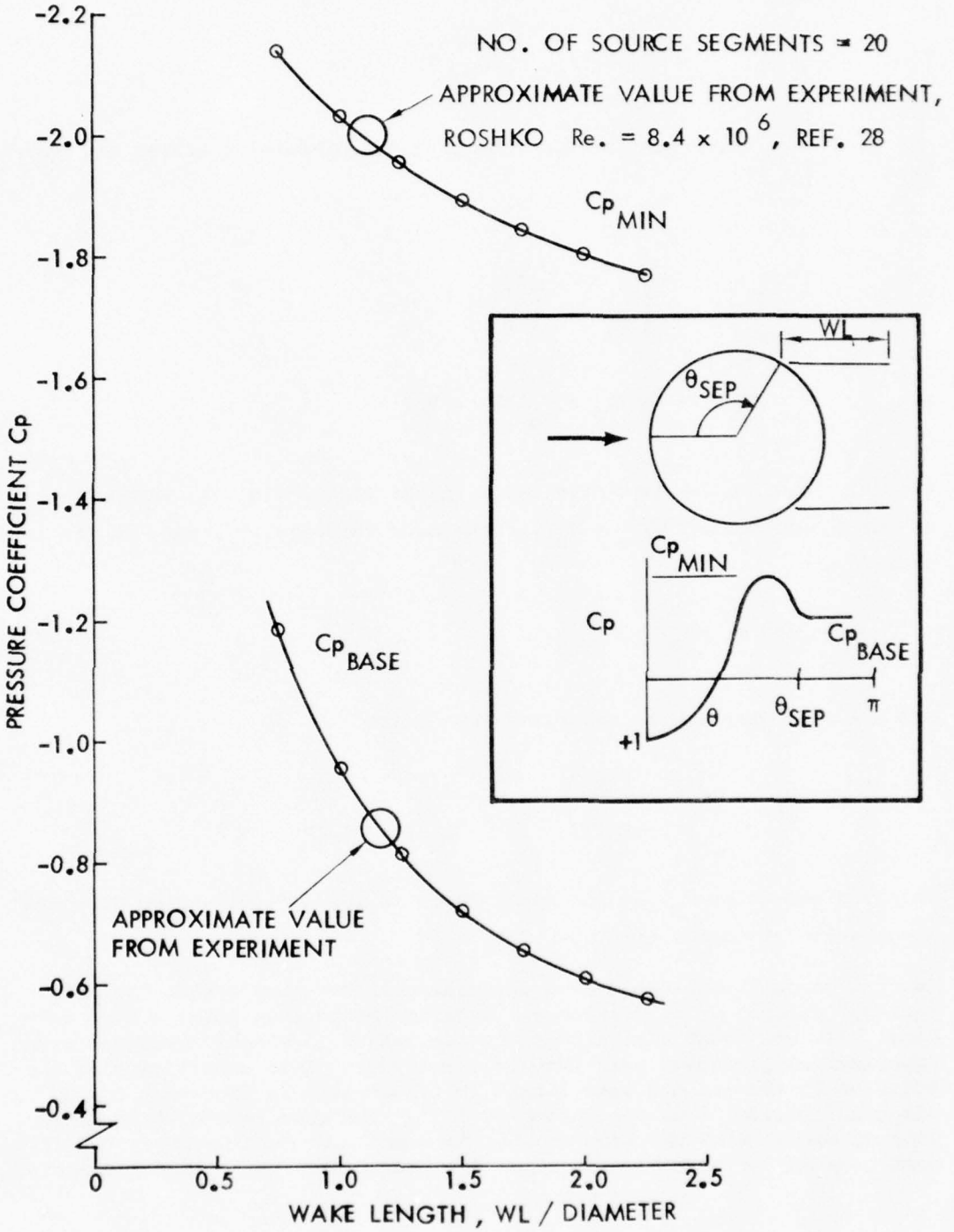

Figure 8. Base Pressure and Peak Suction on a Circular Cylinder as a Function of Wake Panel Length.

Since the "correct" wake length is not generally known a priori, the problem is now a nonlinear one. However, it was observed that the "correct" wake length produced essentially a constant pressure distribution along the outer edge of the wake panel. It was possible to make the problem linear again by using the constant pressure criterion combined with a multiple segment vortex panel. This required additional control points and equations. Although satisfactory solutions were obtained directly, i.e., without iteration, it was felt that the procedure might not be general enough for application to other shapes since some wake length was still prescribed. An iterative technique was, therefore, developed and tested on the circular cylinder case. This technique used the criterion of zero tangential velocity difference between two points on the wake panel (Figure 9). Over a short distance along the wake, the tangential velocity increases if the wake is too short, and it decreases if the wake is too long. Evaluating the tangential velocity increment for two wake length assumptions (e.g., 1. and 1.5 times the base diameter) enables a wake length to be interpolated, which gives zero velocity increment. The process can be continued, but three iterations are generally sufficient (Figure 10).

The "correct" wake length also gives a small plateau in the normal velocity component distribution (Figure 9). This implies that the choice of the control point location on the wake panel is not critical.

Figure 11 shows the calculated pressure distribution on the circular cylinder, using two panel densities, compared with experimental results for a Reynolds Number of 8.4×10^6 (Reference 28). The separation angle, i.e., 105^0, was prescribed at this stage in the model development. The wake length iteration was stopped after the third pass. The 20-panel case (on half the cylinder) gave very good agreement with the experimental pressure distribution, particularly in the separated region, but there is an "overshoot" in pressure just upstream of the separation point.

The case with only 10 panels also gave excellent agreement with experiment in the separated flow region pressures, but it underestimated the suctions upstream of the separation point.

THREE-DIMENSIONAL METHOD

Testing the Potential Flow Model

The two-dimensional procedure described in the previous subsection was extended to the three-dimensional form and applied to a sphere. In this case, the wake vorticity panels form a cylinder behind the sphere. Initial calculations showed a different behavior in the iterative wake-length procedure from that shown in the two-dimensional case. Therefore, the effect of wake length on base pressure was reevaluated, and the results are

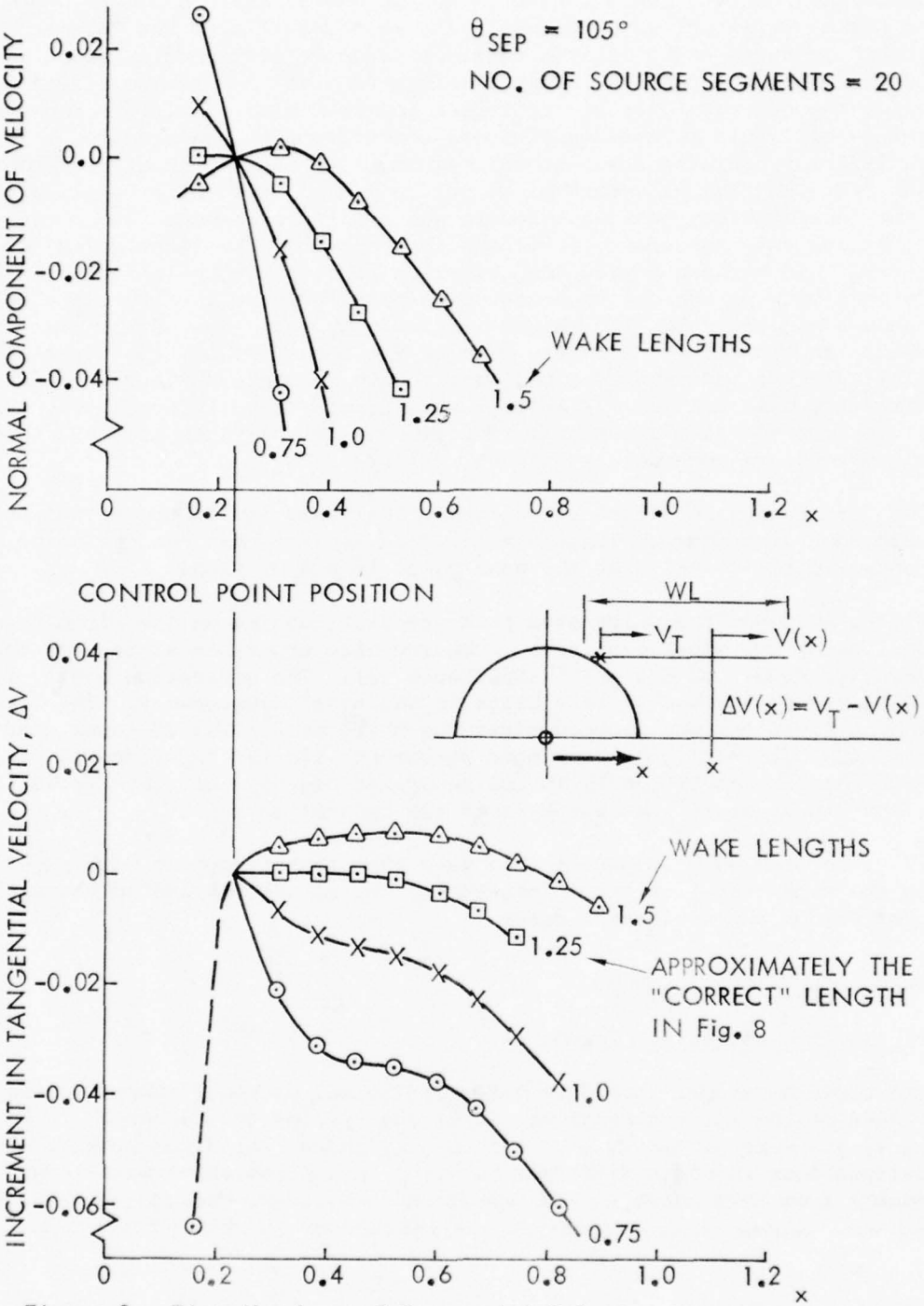

Figure 9. Distributions of Tangential Velocity Increment and Normal Velocity Along the Wake Panel on a Circular Cylinder for Various Wake Lengths.

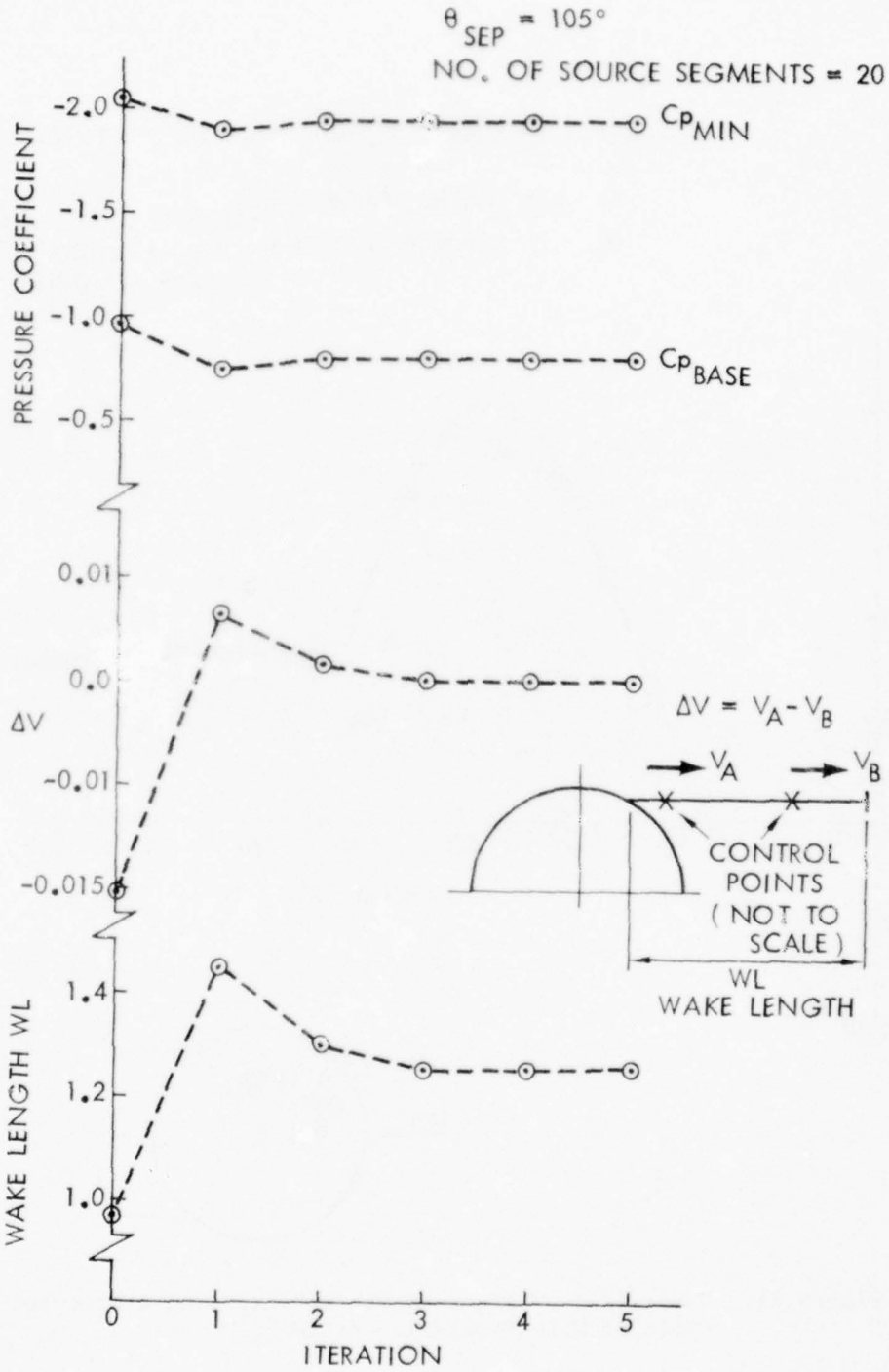

Figure 10. Results From the Iterative Wake Length Procedure Applied to a Circular Cylinder.

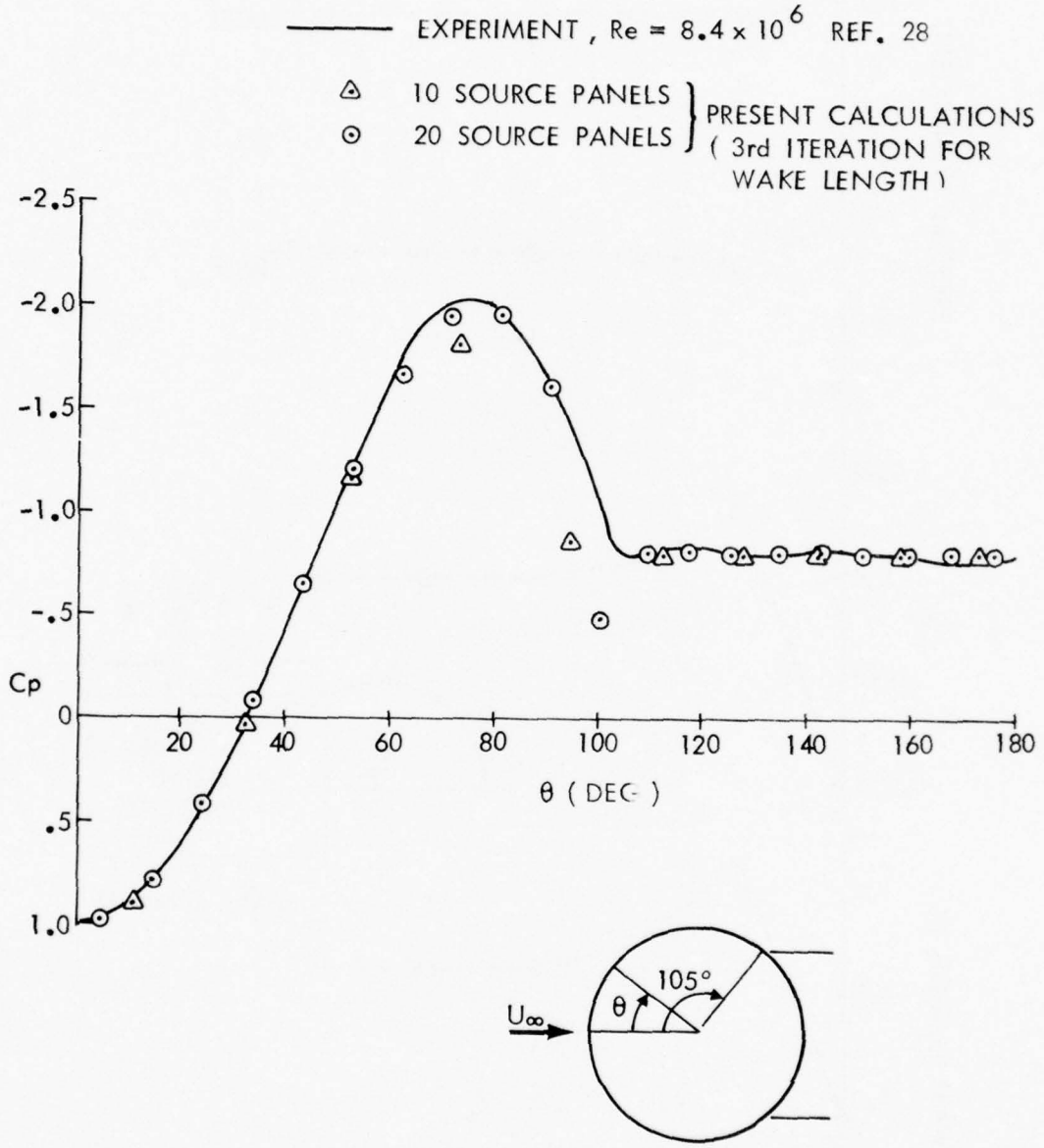

Figure 11. Comparison of Pressure Distributions on a Circular Cylinder With Separation at 105°.

shown in Figure 12 for three prescribed separation angles. The base pressure now appears to have an asymptotic value as wake length increases. It is virtually insensitive to wake length for lengths above about twice the separated wake diameter. The iterative wake length procedure, which was found to be necessary in the two-dimensional case, is evidently not required in the three-dimensional case.

Figure 13 shows the variation of the calculated base pressure on the sphere with a prescribed separation angle. The calculated values are enclosed lines representing wake lengths of one separated-wake diameter and essentially infinity. The enclosed region is not very wide, particularly at the larger separation angles (i.e., higher Reynolds numbers). Two experimental points are included from Reference 29 for Reynolds numbers $.425 \times 10^6$ and $.157 \times 10^6$. In view of the difficulty in obtaining the separation point from the experimental results, the agreement between the theoretical model and experiment is remarkably good.

The rapid variation in base pressure with separation angle, Figure 13, will pose a problem with the present theoretical model in that the necessary displacement of the wake panels from the separation line to the nearest source panel edge will cause a change in predicted base pressure. This might eventually lead to a requirement of a more flexible model that is not constrained to follow panel edges.

FEATURES OF THE COMPLETE PROCEDURE

The full potential flow/viscous flow iterative procedure described earlier was investigated next. The separation points, instead of being prescribed as in the previous subsection, are now calculated in the boundary layer procedure based on the previous potential flow pressure distribution along calculated streamlines. Preliminary calculations highlighted several problems which required some restrictions to be applied to the method. These are described below.

"Rectangular" Paneling Arrangement

The paneling of the surface containing the separated region must form a rectangular grid at this stage; i.e., the number of rows in each column must be constant from the start of the body to a station well downstream of the expected separation line. This restriction is necessary at this stage for the streamline calculation procedure and for the procedures which find the "separation" panels and which redistribute the boundary layer sources and skin friction drag. The procedure that subtracts ΔH from pressures on panels downstream of the separation line in the "rectangular" paneling region also relies on this restriction. It would be possible to develop more general procedures to take advantage of the arbitrary paneling facility of the WBAERO program, but such procedures would be considerably more

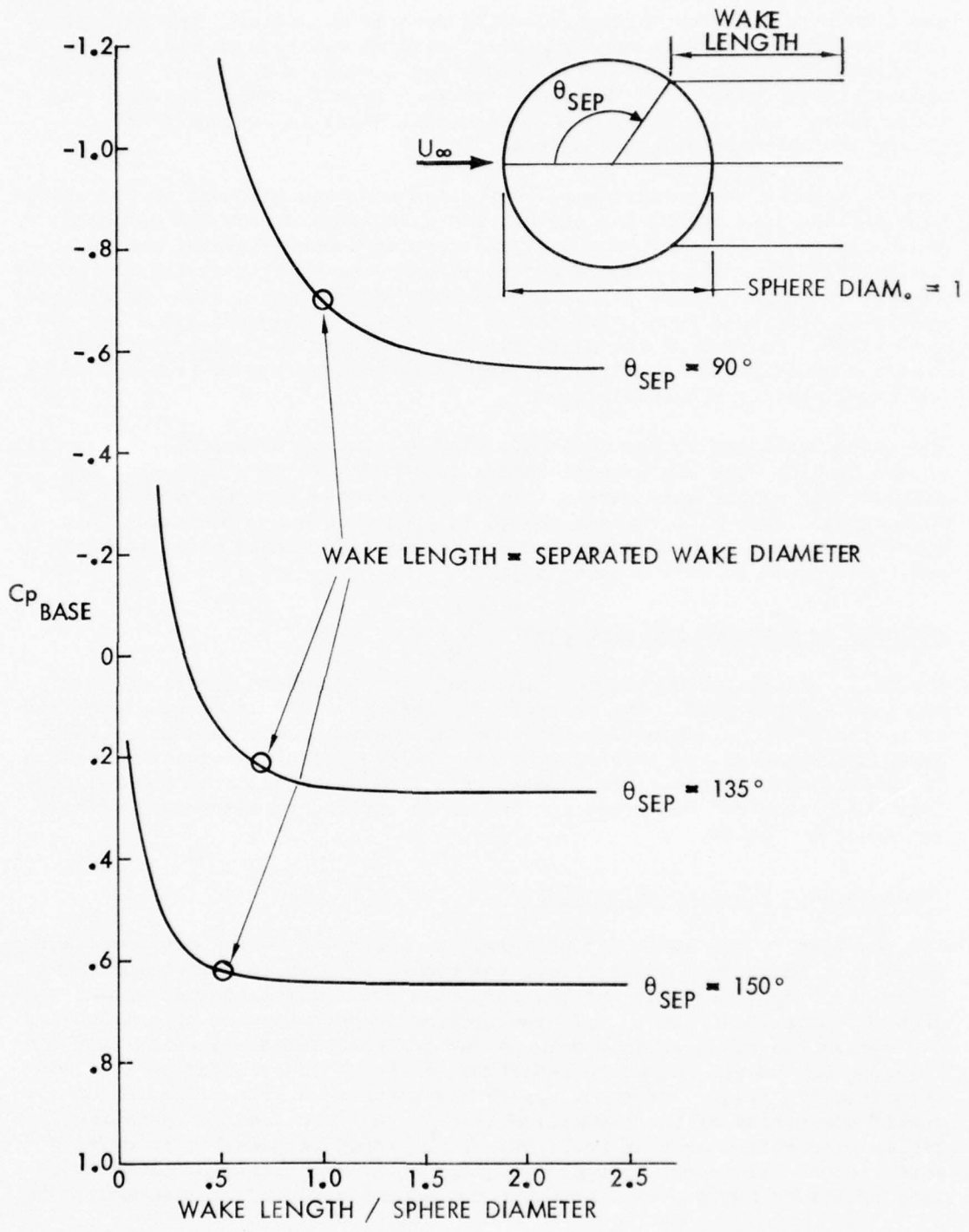

Figure 12. Effect of Wake Length on Calculated Base Pressure on a Sphere for Three Separation Angles.

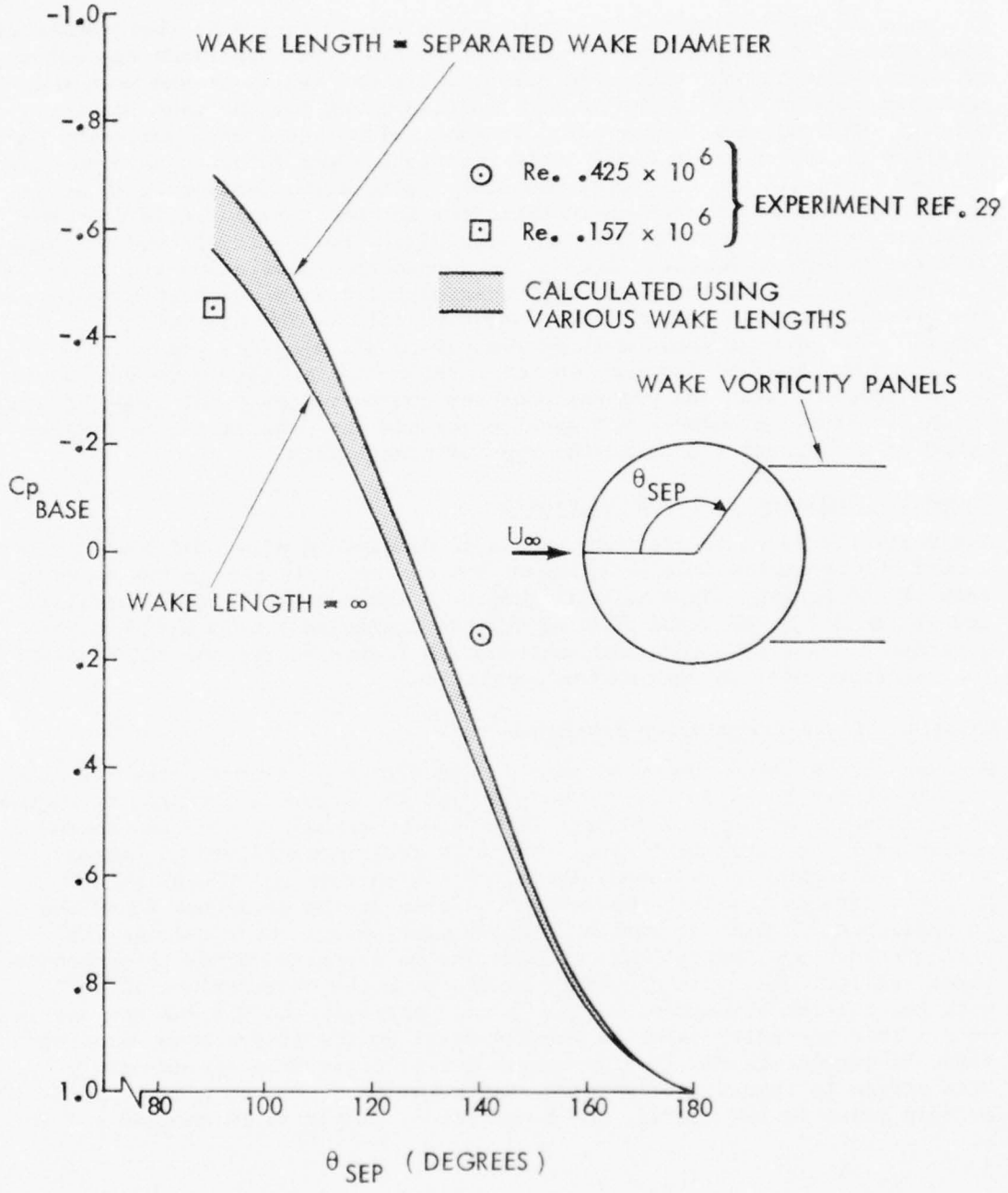

Figure 13. Effect of Separation Angle Base Pressure on a Sphere.

complicated. At this stage of the development of the wake model, the simple "rectangular" scheme is adequate.

The Separation "Line"

The wake paneling program finds the surface panels that have their upstream edge nearest to the predicted separation points. It then finds the column of panels that has the most separation panels defined in it and uses the upstream edge of that column as the starting point for the wake vorticity panels. Each surface source panel in that column has a wake vorticity panel attached to its upstream edge. This restriction was found to be necessary because breaks in the vorticity paneling give distorted vorticity solutions and poor convergence characteristics in the iterative solution procedure. Such breaks occur when the vorticity paneling is allowed to "jump" from one column to another in order to represent a separation line that is inclined relative to the paneling. This restriction can result in a poor representation of the separation line, particularly in angle of attack cases. The problem would only be removed by allowing the separation panels to be attached anywhere on the surface panels. Such a feature would not be possible with the present constant source/vortex panel model because of the interaction between the panel edges and the control points and because of the abrupt change in the type of singularity.

Boundary Condition on the Wake Panels

The vorticity level on the wake panels is determined after the boundary condition of streamwise flow is added on the control points near the upstream edge of the panels. This is analogous to a Kutta trailing-edge condition, and it can force the local flow to deviate appreciably from the real flow direction. This is a possible contributing factor to the low calculated peak suction just upstream of the separation.

Solution of the Singularity Strengths

Because of the large number of panels needed to represent a body, iterative techniques are favored for the solution of the source and vortex strengths. Unfortunately, because of adverse interference between source and vortex panels near the separation line, iterative techniques failed to converge. A modified technique was used, therefore, which combines iterative and direct solutions. This is basically the same as the procedure described in Reference 3; but the direct solution part covers the vorticity and part of the source partitions, so that the main source/vortex interference terms are included. The procedure starts with the Gauss-Seidel method with the initial assumption of zero source strength and 0.1 for the vorticity. (The vorticity value is roughly equal to the free-stream velocity since it represents the jump in tangential velocity from approximately free stream to approximately zero. The solution evaluates $\gamma/4\pi$.) At a certain point in the matrix, the Gauss-Seidel procedure is stopped and

a direct solution performed for the remaining equations. The basic equations are of the form:

$$\sum_{k=1}^{N} A_{jk}\,\sigma_k + \sum_{k=1}^{M} B_{jk}\,\gamma_k = C_j; \qquad j = 1, 2, \ldots, N + M$$

This differs from the two-dimensional form (Equation (63)) in that there are now M wake panels instead of 1. If the Gauss-Seidel operation is taken up to j = m, say, then for the rest of the equations we can write

$$\sum_{k=1}^{M} A_{jk}\,\sigma_k + \sum_{k=m+1}^{N} A_{jk}\,\sigma_k + \sum_{k=1}^{M} B_{jk}\,\gamma_k = C_j;$$

$$j = m + 1, m + 2, \ldots, N + M$$

Using the present Gauss-Seidel solution for σ_k, k = 1, 2, ..., m, the first term can be evaluated and combined with the right-hand side for all of the remaining equations. This leaves a square system of equations which is solved by a direct method. The direct solution for σ_k, k = m + 1, m + 2, ..., N, and for γ_k, k = 1, 2, ..., M is then used for the next pass through the Gauss-Seidel procedure and so on. Currently, the direct solution is performed for the last 140 equations, which adequately covers the region of close interaction between the source and vortex panels. The procedure typically converges within six iterations for a residual limit of 10^{-3}. If the number of unknowns is less than 141, then the whole solution is by the direct method. The attached flow solution, which involves source panels only, is always obtained by the unmodified Gauss-Seidel technique.

Boundary Layer Source and Skin Friction Distribution

Boundary layer source values and skin friction values are known only along each streamline. Because the panel history is known along each streamline, the source and skin friction values can be set on those panels crossed by streamlines. The values on other panels are set by interpolation down each column. Downstream of the separation line, the boundary layer source and skin friction values are set to zero.

CALCULATION AND DISCUSSION OF RESULTS

SPHERE CASE

A sphere calculation using 112 panels was performed for a Reynolds Number of $.425 \times 10^6$. The resulting pressure distribution for two iterations is shown in Figure 14 together with an experimental distribution from Reference 29. Also included are the exact and calculated attached flow pressure distributions. The first iteration result shows a later separation angle than the experiment and a higher base pressure; i.e., $C_{p_{BASE}}$ is .3 instead of .1. The second iteration shows an earlier separation than the experiment and a lower base pressure; i.e., C_p is .02 instead of .1. Further iterations were not attempted at this stage because it is suspected that earlier calculated separation is being forced after the first iteration because of the positive pressure overshoot just upstream of the wake model vorticity panels (Figure 14). This augments the adverse pressure gradient over the rear of the body. Both iterations show a loss in peak suction on the sphere (Figure 14). A factor which may be causing the reduced peak suction and also the positive pressure overshoot is the boundary condition that forces the flow to be stream-wise just after separation. An improved boundary condition for the wake panels might, therefore, be necessary.

B0105 FUSELAGE CASES

The method was applied to the B0105 fuselage using two paneling arrangements. The first case had 72 panels. The "rectangular" paneling region had 6 rows by 10 columns and covered the main part of the fuselage and the start of the boom (Figure 15). The second case had 241 panels (Figure 16) with 9 rows by 25 columns on the "rectangular" paneling area. The calculated pressure distributions along waterline 6 (Figure 16) for the two paneling schemes are compared in Figure 17 for the second potential flow/viscous flow iteration. This clearly demonstrates the need for fairly dense paneling to define the peak suction areas adequately. Both distributions show the positive pressure overshoot just upstream of the separation that was observed in the sphere and cylinder cases.

Figure 18 shows the calculated streamlines from the dense paneling case for two iterations. The starting points for the streamline calculations were in the column of panels at x-station 36.5. The changes in the streamline paths are fairly small, and the calculated separation points on each streamline are in good visual agreement with experimental observations (Reference 2).

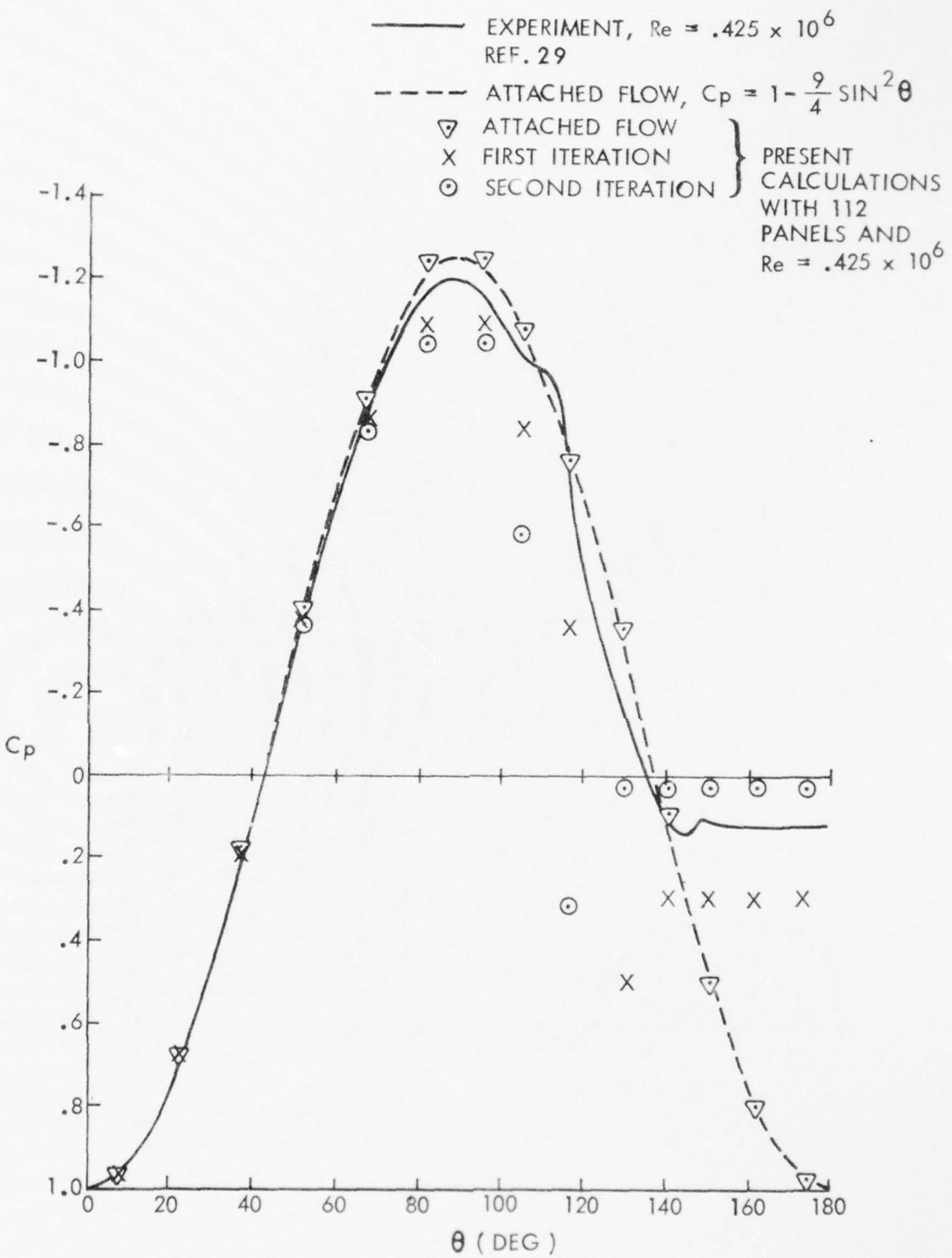

Figure 14. Comparisons of Pressure Distributions on a Sphere.

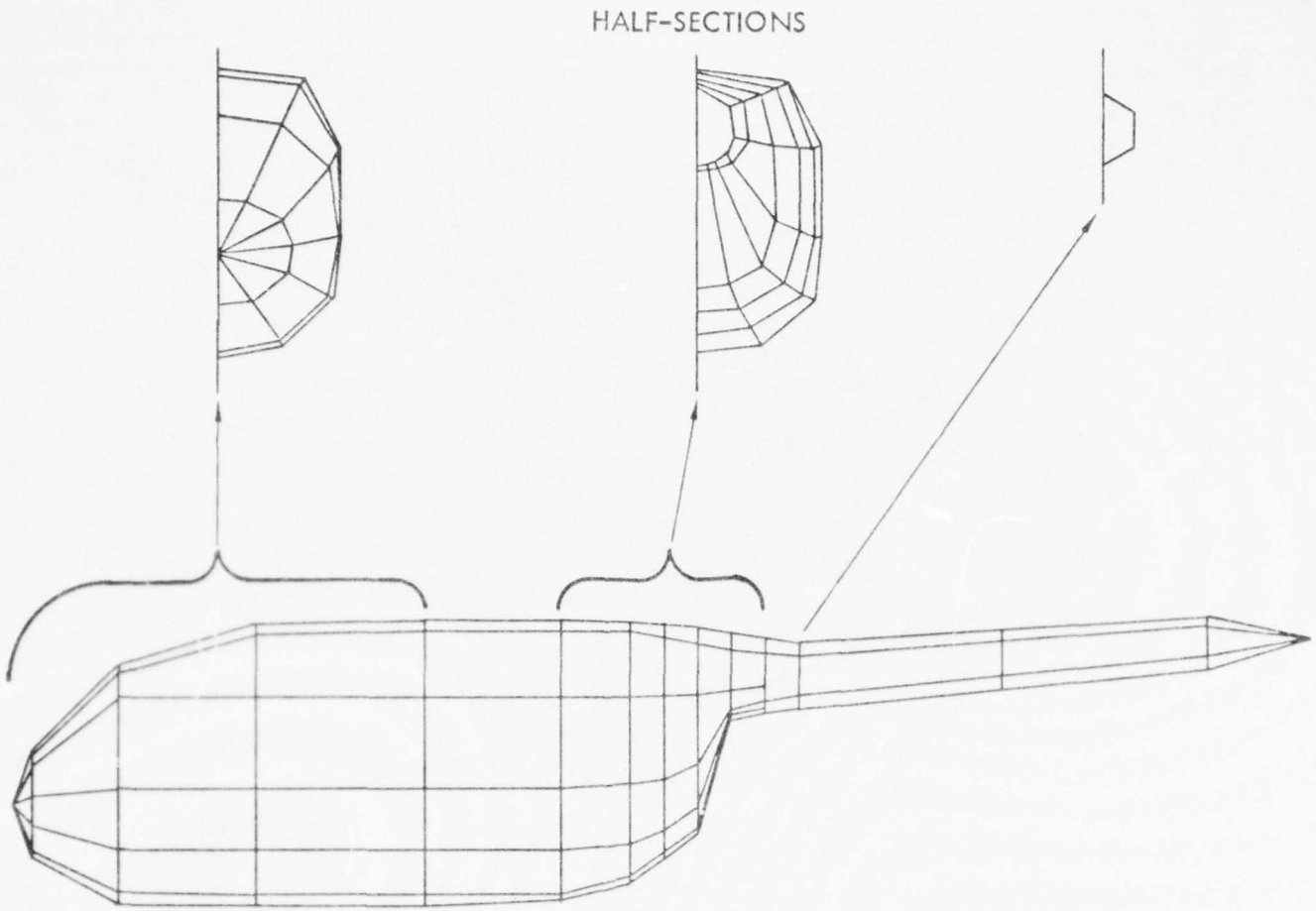

Figure 15. Panel Arrangement on the B0105 Fuselage and Boom - 72-Panel Case.

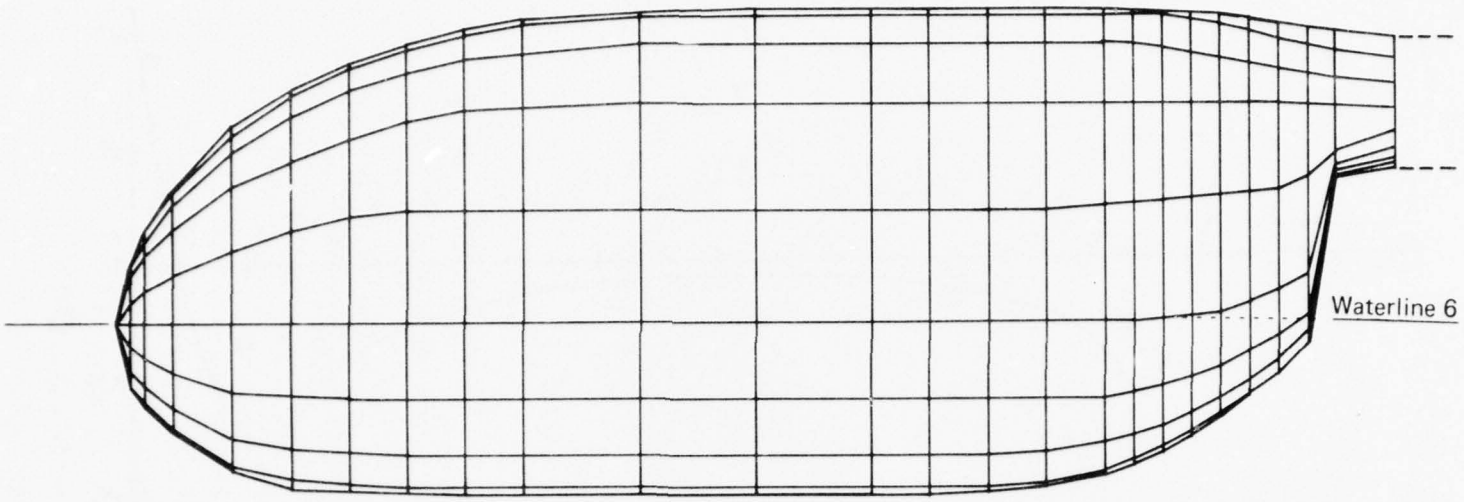

Figure 16. Side View of the 241-Panel Arrangement on the BO105 Fuselage.

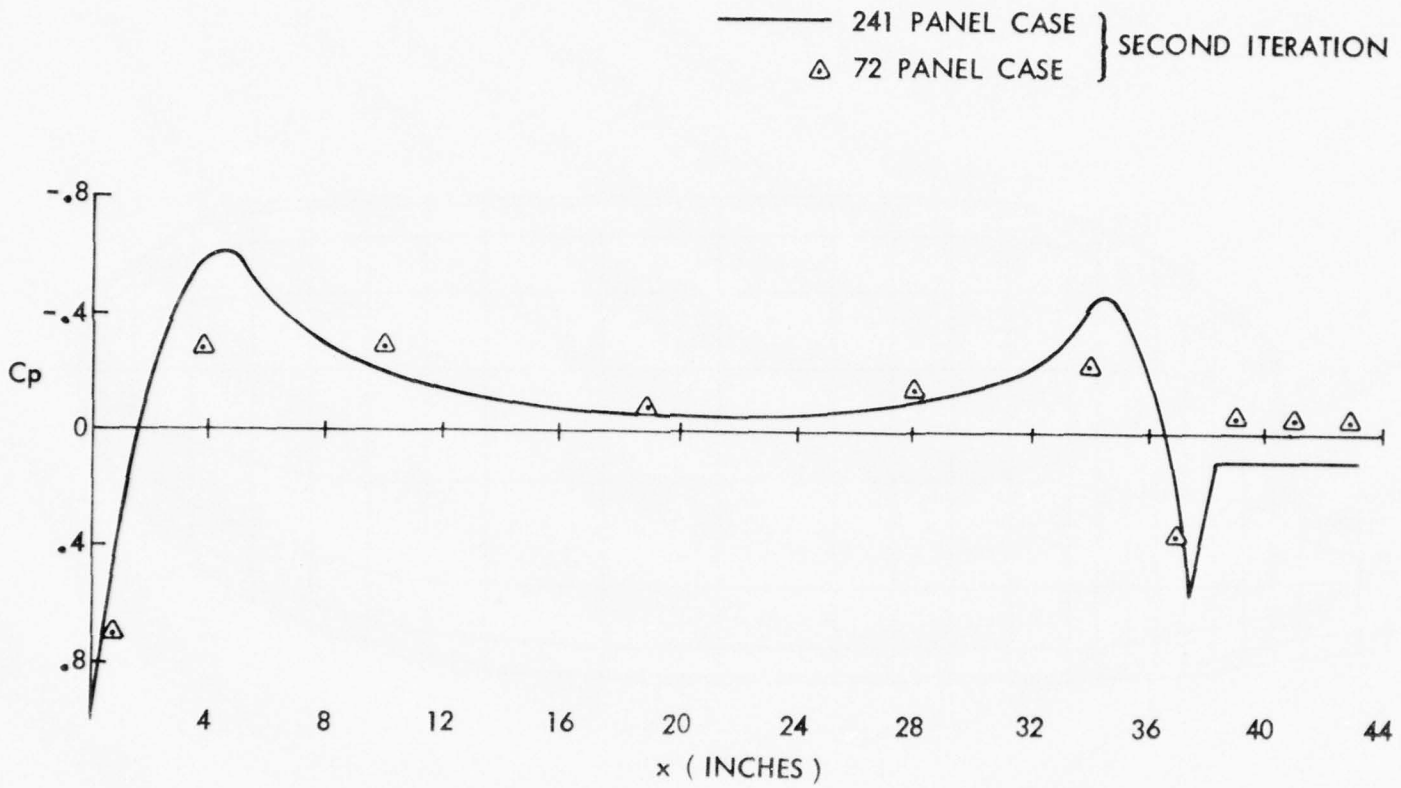

Figure 17. Effect of Panel Density on the Calculated Pressure Distribution Along Waterline 6 on the B0105 Fuselage.

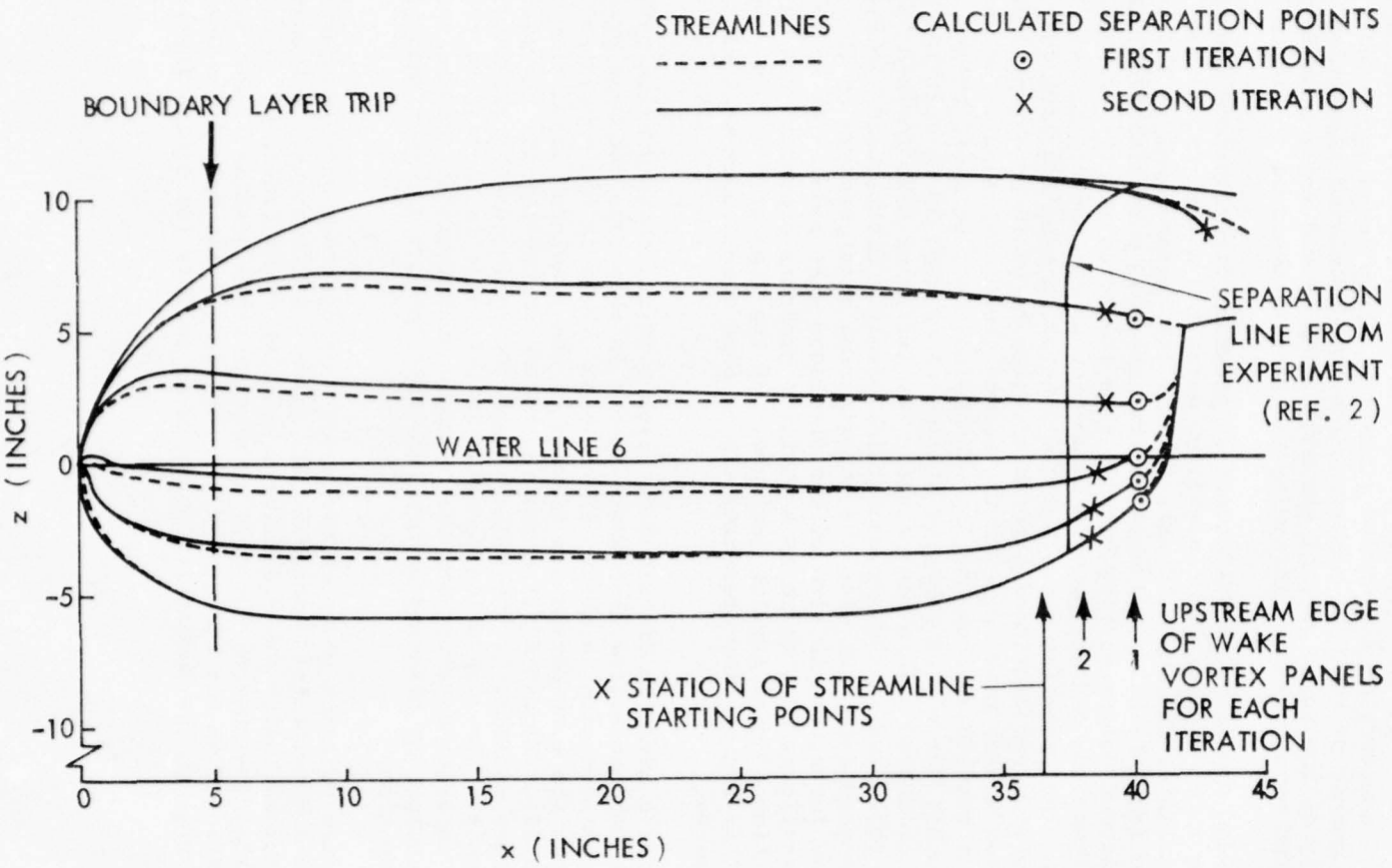

Figure 18. Calculated Streamlines and Separation Points on the BO105 Fuselage for Two Iterations (241-Panel Case).

The starting points for the wake vortex panels (Figure 18) show a reasonable representation of the separation line for the first iteration, except on the top surface of the body where the calculated separation line moves downstream. However, on the second iteration, there is an appreciable forward displacement of the wake paneling from the calculated separation line, particularly on the upper part of the body. This would imply a shift in the predicted base pressure, following the results observed in Figure 13.

Calculated and experimental (Reference 2) pressure distributions are compared along three lines: top centerline, waterline 6 (see Figure 18), and bottom centerline, in Figure 19 (a), (b) and (c), respectively. The calculations are from the 241-panel case and the attached potential flow, the first and second potential flow/viscous flow iteration results are presented. The first iteration did not predict separation on the top of the body within the "rectangular" paneling area, but the separation paneling from the lower part of the body was continued onto this region to avoid an abrupt change in the vortex/source paneling. On the second iteration, separation was predicted at station 42.8 on the top streamline; but, to avoid breaks in the wake model, the vortex paneling started at station 38 to suit the majority of the predicted separation points. The effect of this forward "separation" is reflected in the top centerline pressure distribution in Figure 19(a). The good agreement with the experimental base pressure on this line is, perhaps, fortuitous in view of the displaced wake model. As in the sphere case (figure 14), there is a positive pressure overshoot and an underprediction of peak suction just ahead of the separated region. Upstream of this region, the pressures are in good visual agreement within the experiment.

The waterline 6 pressure distribution, Figure 19(b), shows similar tendencies to the top centerline distribution, but in this case the base pressure on the second iteration is about .17 too high. This is not consistent with the fact that the wake panels are forward of the predicted separation line (see Figure 13). Figure 19(c) shows the bottom centerline distributions. Here, the base pressure at the second iteration is in good agreement with the experiment. The separation paneling in this case is closest to the calculated separation points and the pressure distributions compare reasonably well except, as observed before, the calculations underestimate the rear peak suction.

The calculated positive pressure overshoot just upstream of the separation paneling is a detrimental feature in all three distributions. Not only does this automatically cause earlier separation to be predicted on the next iteration (because of the more adverse pressure gradient), but it has a large influence on the integrated pressure drag. The calculated drag breakdown, D/q, at the second iteration is as follows (in square feet):

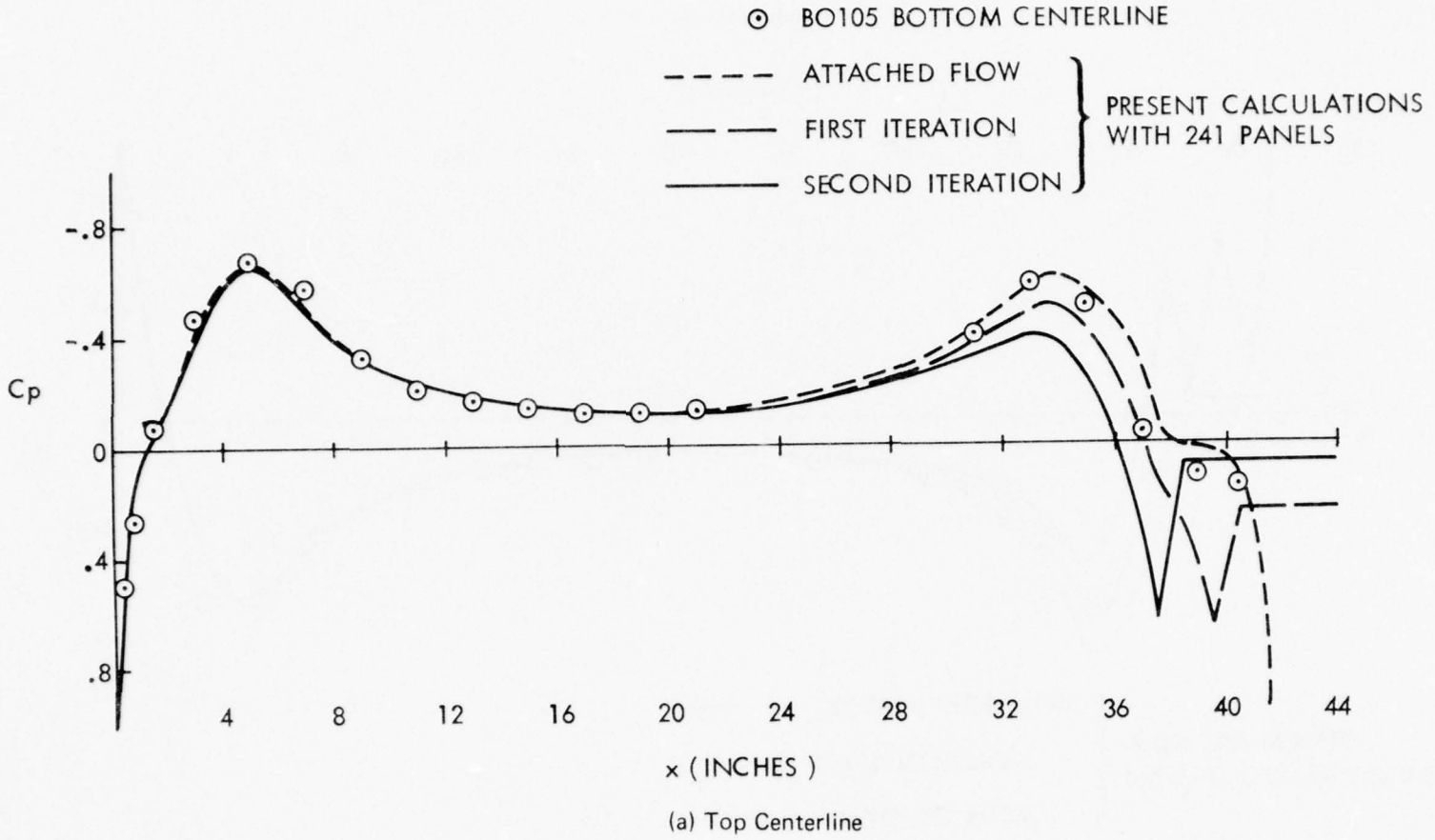

(a) Top Centerline

Figure 19. Comparison of Calculated and Experimental Pressure Distributions on the BO105 Fuselage.

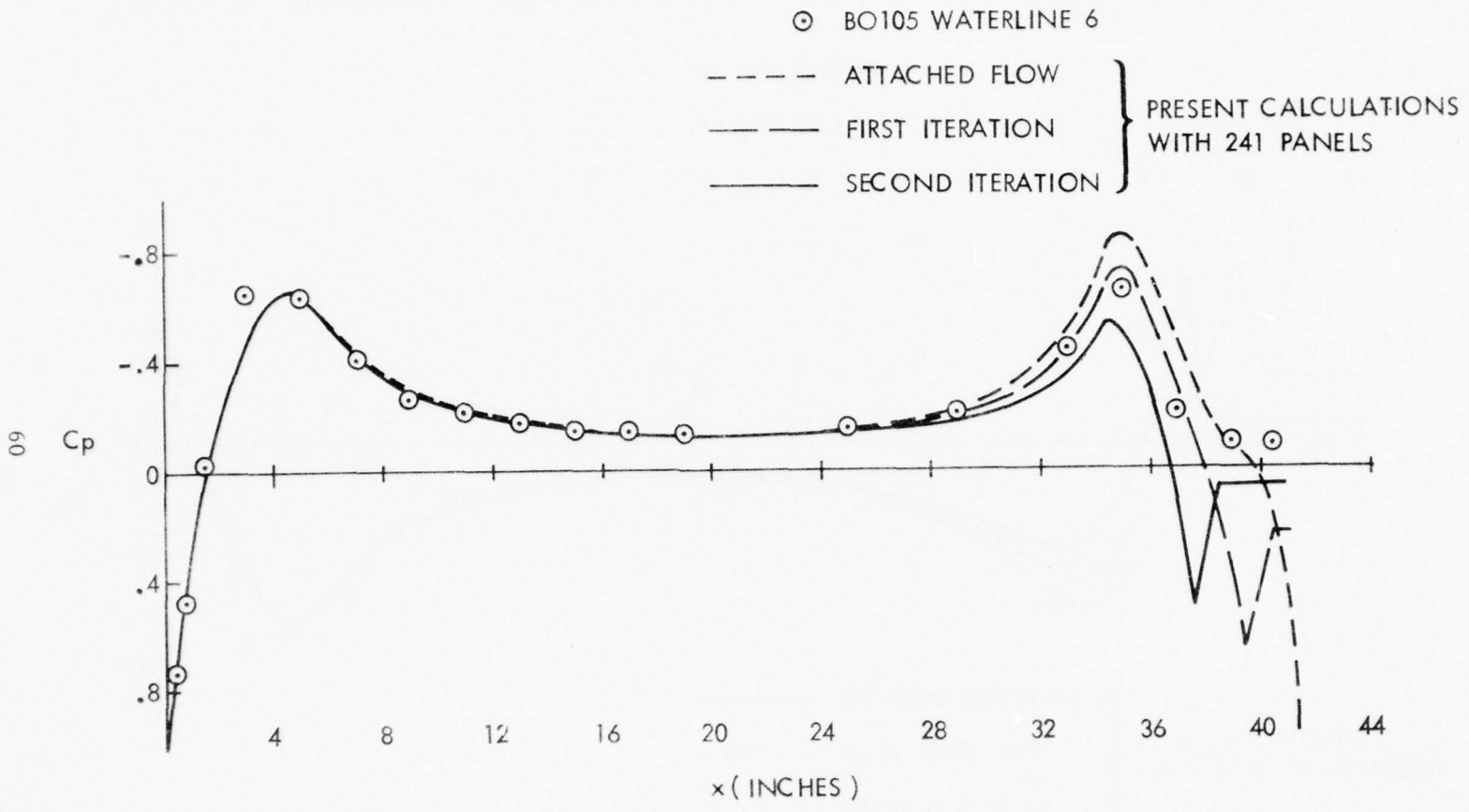

(b) Waterline 6

Figure 19. Continued.

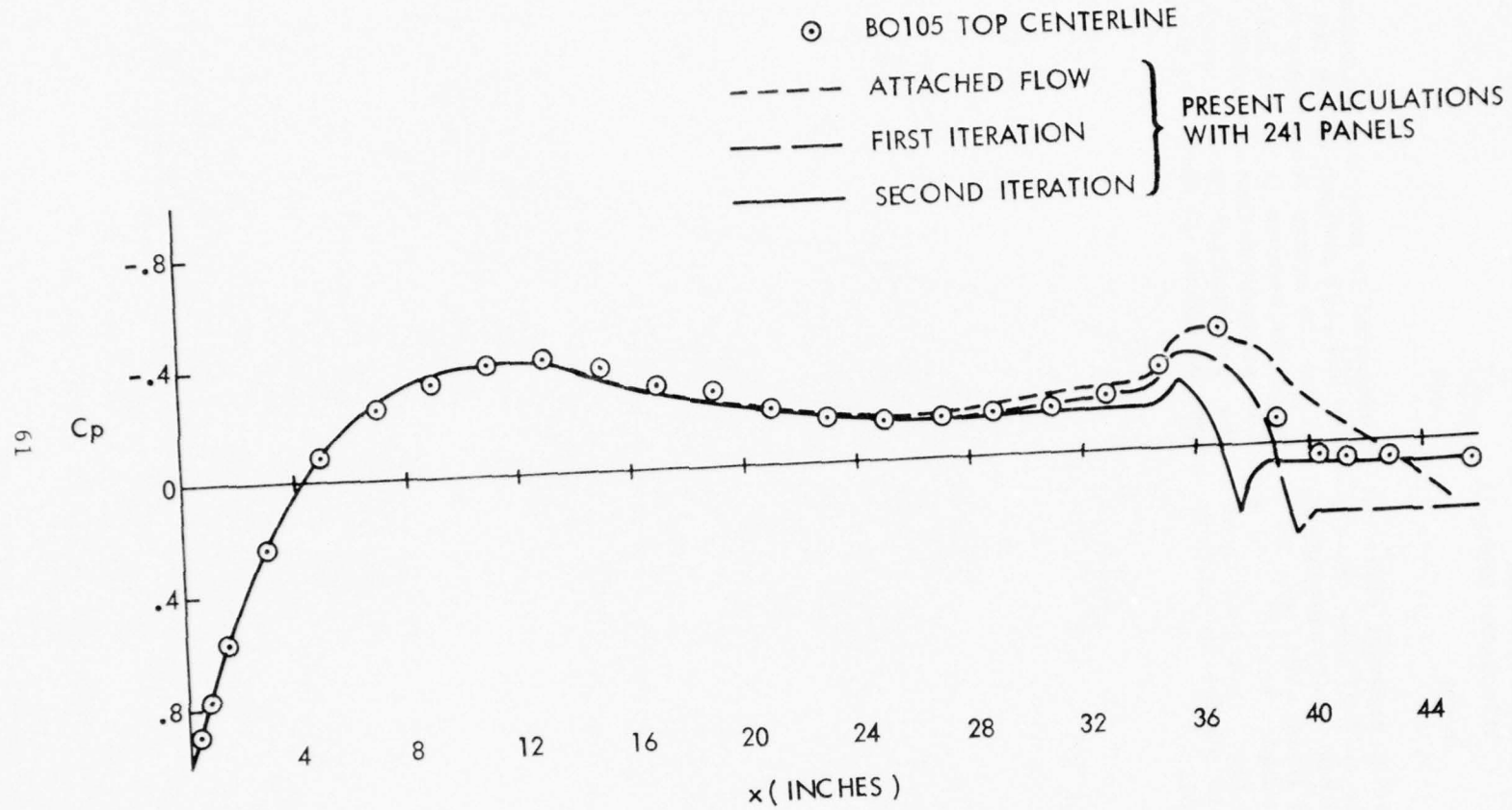

(c) Bottom Centerline

Figure 19. Concluded.

Skin Friction	.045
Integrated Pressure	-.087
Total	-.042

The positive pressure overshoot is estimated to have lost approximately .1 square foot of D/q. Base pressure and peak suction errors are estimated to have lost approximately .07 and .04 square foot respectively. The boom gives additional small drag errors because it is not fully treated at this stage. Strictly, ΔH should be subtracted from all panels inside the wake (i.e., not just those in the "rectangular" paneling area), but this would require an extensive search procedure to check the geometry of each panel.

CONCLUSIONS

1. The separated flow model has demonstrated reasonable accuracy in the predicted surface pressures upstream of the separation line with fair agreement in base pressure. However, improvements are needed in the rear peak suction regions and the positive pressure overshoot just upstream of the separation line should be removed.

2. Certain improvements are needed in the model to allow more flexibility in the wake paneling. A more accurate representation of the separation line is required, rather than moving the wake panels to the nearest source panel edges. Such an improvement should result in more accurate predictions of base pressure.

3. The calculated streamlines and separation points are in good visual agreement with experimental observations.

SUGGESTED PROGRAM IMPROVEMENTS

The detrimental features of the source/vortex panel model can be largely removed by going to a vorticity panel method. Such a method has been developed very recently for predicting lift coefficients beyond the stall in two-dimensional flow. Applied to the drag prediction problem, the vorticity model would have surface panels of linearly varying vorticity (Figure 20). The wake vorticity panels would be similar to those in the present work, but the vorticity level would be the same as the value on the surface panel at the attachment point. The "Kutta" condition can be applied which makes the lower vorticity panel to be equal but opposite to the upper one; this feature would extend the present method to allow lifting cases to be considered. Inside the separated wake region, vorticity is constrained to be zero just downstream of the separation points; the rest of the corner vorticity values in between are evaluated in the solution. Boundary conditions, therefore, are applied only on the body surface; hence, the wake panel boundary points of the source/vortex model are eliminated. This feature contributes to an improved prediction of upstream suction; e.g., in the cylinder case, 12 vorticity panels give very good comparison with the experimental pressure distribution (Figure 21). They are equivalent to 20 source panels and yet do not show the positive pressure overshoot. Positive pressure "overshoots" and "undershoots" have been obtained from the vorticity model when using a large number of panels on an airfoil. Correct wake orientation seems to be the answer to this problem, and a relaxed wake procedure might be called for eventually.

With the surface vorticity model, the vorticity is continuous, moving from the surface onto the wake panel. There are no abrupt changes in singularity strength or type. Arbitrary wake paneling is, therefore, possible; i.e., the wake panels can be attached along any line on the surface panels. Accurate representation of the separation line would, therefore, be possible, with this model. This would remove the problems associated with the source/vortex wake paneling restrictions. In addition, the vorticity continuity feature would allow the separation modeling to finish in the middle of a surface - the vorticity would simply stay on the surface where separation is not predicted. Because of the continuity, numerical solution of the equations should be better behaved than in the case of the source/vortex model.

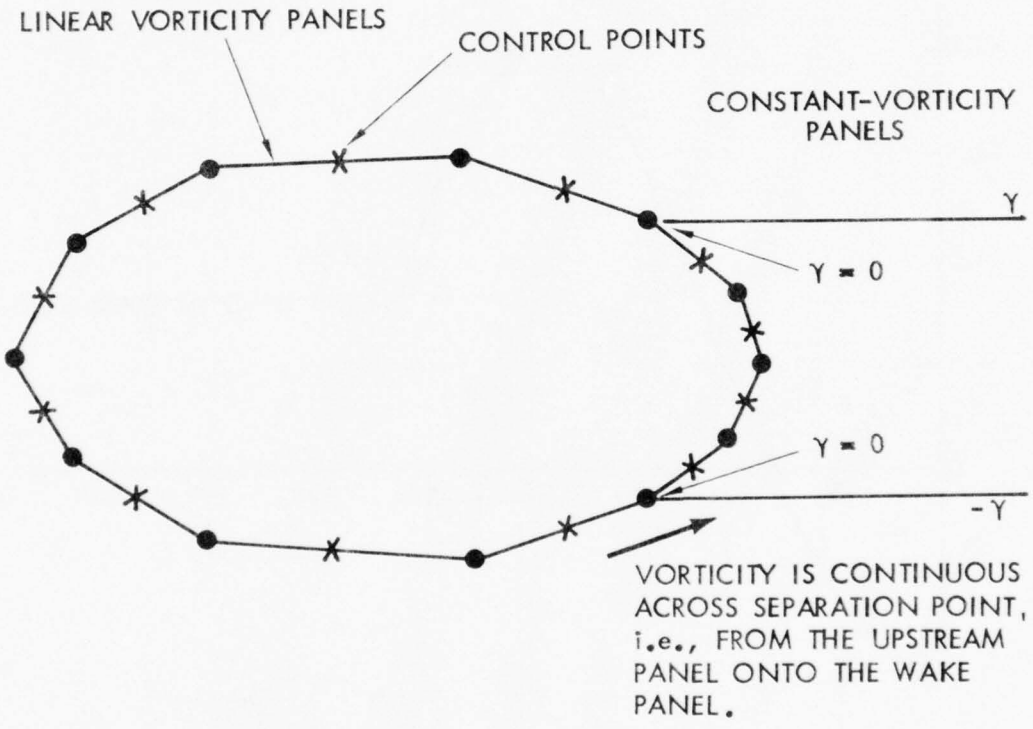

Figure 20. Separated Flow Model Based on Vorticity Panels.

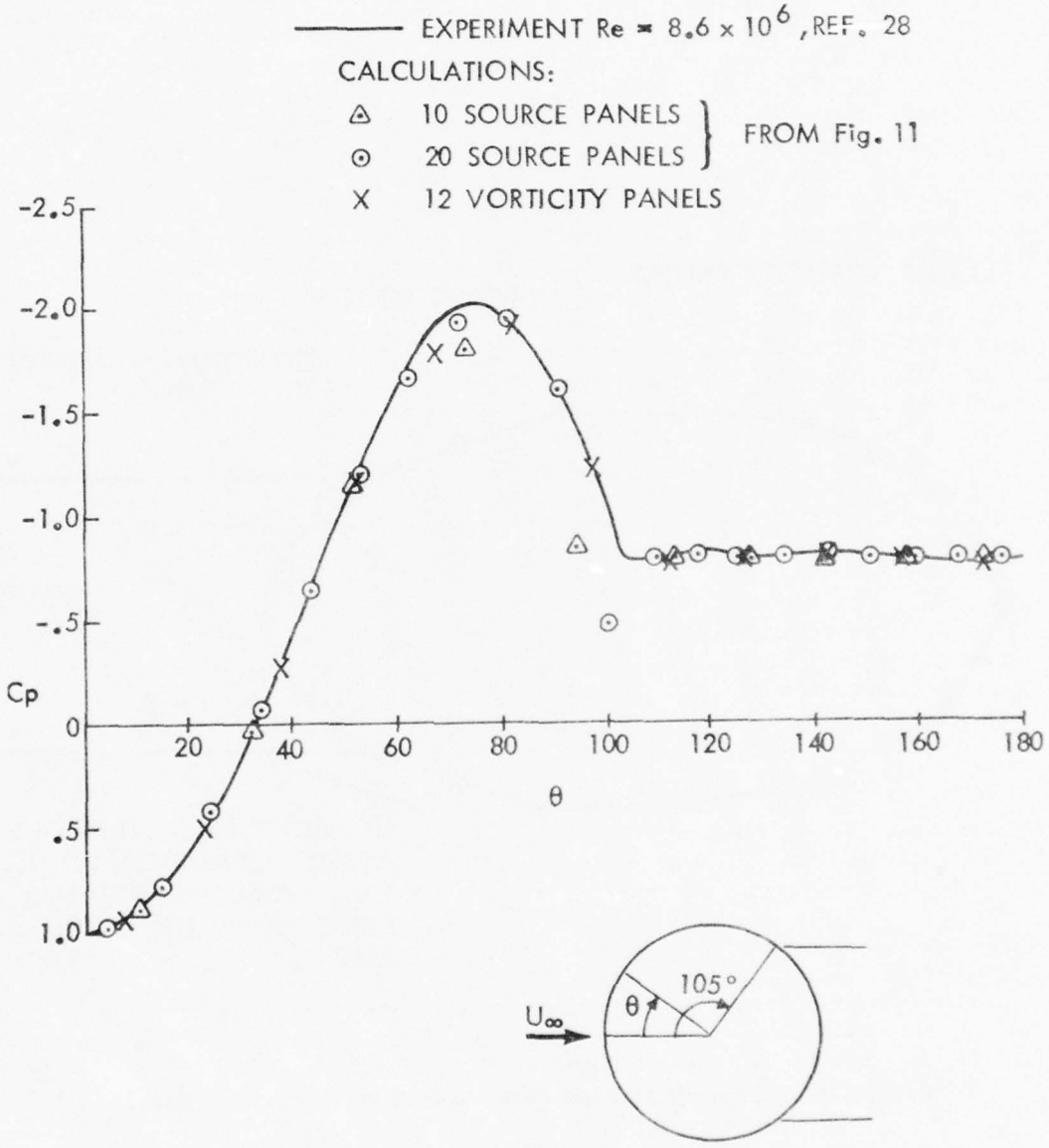

Figure 21. Pressure Distribution on a Circular Cylinder Calculated by a Surface Vorticity Method. Comparison With Previous Distribution From Figure 11.

REFERENCES

1. Chapman, D.R., Mark, H., and Pirtle, M.W., "Computers vs. Wind Tunnels for Aerodynamic Flow Simulations", Astronautics and Aeronautics, pp. 22-30 & 35, April 1975.

2. Gillespie, J., "An Investigation of the Flow Field and Drag of Helicopter Fuselage Configurations", Twenty-ninth Annual Forum of the American Helicopter Society, May 1973.

3. Woodward, F.A., Dvorak, F.A., and Geller, E.W., "A Computer Program for Three-Dimensional Lifting Bodies in Subsonic Inviscid Flow", Flow Research, Inc.; USAAMRDL Technical Report 74-18, Eustis Directorate, U.S. Air Mobility Research and Development Laboratory, Fort Eustis, Virginia, April, 1974, AD 782202.

4. Anon., "Fuselage Geometry Definitions Program", Sikorsky Aircraft Report SER 50866.

5. Hess, J.L., and Smith, A.M.O., "Calculation of Potential Flow about Arbitrary Bodies", Progress in Aeronautical Sciences, Vol. 8, 1967.

6. Rubbert, P.E., Saaris, G.R., et al., "A General Method for Determining the Aerodynamic Characteristics of Fan-in-Wing Configurations, Volume I: Theory and Application", The Boeing Co., USAAVLABS TR 67-61A, December 1967, AD 667980.

7. Dawson, C.W., and Dean, J.S., "The Calculation of Streamline Data for Boundary Layer Input", NSRDC CMD-4-74, January 1974.

8. Nash, J.F., "The Calculation of Three-Dimensional Turbulent Boundary Layers in Incompressible Flow", J. Fluid Mechanics, 37, 1969.

9. Bradshaw, P., "Calculation of Three-Dimensional Turbulent Boundary Layers", J. Fluid Mechanics, Vol. 46, 1971.

10. Spalding, D.B., Imperial College, London, Private Communication, Sept. 1974.

11. Curle, H., "A Two Parameter Method for Calculating the Two-Dimensional Incompressible Laminar Boundary Layer", J.R. Aero Soc., Vol. 71, 1967.

12. Thwaites, B., "Approximate Calculation of the Laminar Boundary Layer", Aero Quart., Vol. I, 1949.

13. Rott, N., and Crabtree, L.F., "Simplified Laminar Boundary Layer Calculations for Bodies of Revolution and for Yawed Wings", Journal of Aeronautical Sciences, 19, 553, 1952.

14. Granville, P.S., "The Calculation of the Viscous Drag of Bodies of Revolution", David W. Taylor Model Basin Report 849, 1953.

15. Schlichting, J., and Ulrich, A., "Zur Berechnung Des Jnsellages Laminar-Turbulenten" (On the Calculation of Laminar-Turbulent Transition), Jahrbuch 1942 Der Deutschen Luftfahrt-Forschung.

16. Smith, A.M.O., "Transition, Pressure Gradient and Stability Theory" Proc. 9th Internat. Congress of Appl. Mech., Brussels, Vol. 7, 1957.

17. Coles, D.E., "Measurements in the Boundary Layer on a Smooth Flat Plate in Supersonic Flow", Jet Propulsion Lab Report No. 20-69, 1953.

18. Briley, W.R., "An Analysis of Laminar Separation - Bubble Flow using the Navier-Stokes Equations", Proceedings - Fluid Daynamics of Unsteady, Three-Dimensional and Separated Flows, Georgia Tech., June 1971.

19. Gaster, M., "The Structure and Behavior of Laminar Separation Bubbles", ARC 28-226, 1967.

20. Kline, S.J., Morkovin, M.V., Sovran, G., and Cockrell, D.J., "Computation of Turbulent Boundary Layers", Proceed. 1968 AFOSR-IFP Stanford Conference, Stanford University Press, Stanford, Calif., 1969.

21. Nash, J.F., and Hicks, J.G., "An Integral Method Including the Effect of Upstream History on the Turbulent Shear Stress", Proceed. Computation of Turbulent Boundary Layers - 1968, AFOSR-IFP-Stanford Conference, Vol. 1, Stanford University Dept. Mech. Eng., Stanford, Calif.

22. Coles, D.E., "The Law of the Wake in the Turbulent Boundary Layer", J. Fluid Mech., Vol. 1, 1956.

23. Nash, J.F., and Macdonald, A.G.J., "A Calculation Method for the Incompressible Turbulent Boundary Layer, Including the Effect of Upstream History on the Turbulent Shear Stress", N.P.L. Aero Report 1234, 1966.

24. McDonald, H., and Stoddart, J.A.P., "On the Development of the Incompressible Boundary Layer", Brit. Aircraft Corp. (Preston) Aero Report AC 223, 1965.

25. Dvorak, F.A., "The Calculation of Turbulent Boundary Layers on Rough Surfaces in Pressure Gradient", AIAA Journal, Vol. 7, No. 9, September 1969.

APPENDIX I. PROGRAM USER'S GUIDE

PROGRAM INPUT DESCRIPTION

Card Set	Input	Format
1.	Case Title	8A10
2.	RNB, TRIPUP, OPTION, TRMAX, XROUGH, REFC, UIN, XGEM	8F10.0
3.	UKU, DEN, XO, EPS, XNROUGH	7F10.0
4.	VRD(1) ... VRD(NROUGH)	7F10.0
5.	XPRINT, XSKIP, REFX, REFZ, CREF, PRINT, CASE	7F10.0
6.	NPANEL, NBX, MBX, NWX, MWX, NVX, MVX, ILX, NPTS	9I5
7.	TEXT Card:- GEOMETRY INPUT	8A10
8.	CASE, PLOT, SIM, ISAVE, PRINT	5I10
9A.	SINGPA, NOPAN	2I10
9B.	X(I), Y(I), Z(I)	7F10.0
9C.	NPAN (1) ... NPAN(NOPAN)	7I10
10A.	NB	I10
10B.	XBE, YBE, ZBE, MB, OPT, FLAG	3F10.0, 3I10
10C.	B(J), A(J), D(J)	7F10.0
10D.	D(J), B(J), A(J)	3F12.0
11A.	NW, KOORD	2I10
11B.	XBE, YBE, ZBE, CHRD, ALF, XAL, MW, OPT, FLAG, DEL	6F10, 4I5
11C.	DELTA, YO, ZO	7F10.0
11D.	B(J), A(J)	7F10.0
11E.	B(J), D(J), A(J), C(J)	5F12.0
12.	WAKE, POINT	7F10.0
13A.	XLP, YLP, ZLP	7F10.0
13B.	XLP, YLP, ZLP	7F10.0
14A.	NV	I10
14B.	XBE, YBE, ZBE, MV, OPT, FLAG, SIMPOT	3F10.0, 4I10
14C.	B(J), A(J), C(J), D(J)	7F10.0
14D1.	A, B, D	7F10.0

26. Dvorak, F.A., "The Calculation of Compressible Turbulent Boundary Layers with Roughness and Heat Transfer, AIAA Journal, Vol. 10, No. 11, November 1972.

27. Head, M.R., "Entrainment in the Turbulent Boundary Layer", R and M 3152, 1958, Aeronautical Research Council.

28. Roshko, A., "Analytical and Experimental Studies on Drag and Flow of Two-Dimensional Bodies", NACA Technical Notes 2913 and 3169, 1953 and 1954.

29. Fage, A., "Experiments on a Sphere at Critical Reynolds Numbers", Aero. Res. Comm. Tech. Rept. R.& M. 17566, September 1936.

Card Set	Input	Format
14D2.	A, B, D	7F10.0
14D3.	A, B, D	7F10.0
15.	TEXT Card:- AERODYNAMIC CALCULATIONS	8A10
16.	NIT, IEPS, ITYPE	3I10
17.	COMPT, SECT	2I10
18.	REFA, REFL, XOO, X25	7F10.0
19.	KUT, NBV, NV(1) ... NV(5)	7I10
20.	KOMPR, POINTS	2I10
21.	NMA	I10
22.	MA	7F10.0
23.	NAL	I10
24.	ALPHA, BETA	7F10.0
25.	IS	I10
26.	IA, IE	2I10
27.	IREI	I10
28.	II(1), II(2) ... ETC.	14I5
29.	DELY, REFL, XLE	7F10.0
30.	TEXT CARD:- STREAMLINE CALCULATIONS	8A10
31.	ENDFILE	I10
32.	NLIN, NSP(1), ... NSP(NLIN)	14I5
33.	6/7/8/9	

Description of Input Variables

Card 1 - General Identification - Card 1 contains any desired identifying information in Columns 1 - 80.

Card 2 - General Parameters

Column	Variable	Value	Description
1-10	RNB	arbitrary	Reynolds number based on reference chord and free-stream velocity $U_\infty C/\nu$ x (10^{-6}) N.B. If the input geometry is in dimensional units, the Reynolds number will be input per unit, i.e., Re/inch.
11-20	TRIPUP	"	Trip location (x/c)
		1.	No tripping desired
21-30	OPTION	0.	Boundary layer will trip where specified by TRIPUP
		1.	Program will test on boundary layer momentum thickness at trip location. If $R_\theta < 200$, trip location will be repositioned to point where $R_\theta \geq 200$. This deters the user from specifying an unrealistically early trip location
31-40	TRMAX	arbitrary	Maximum number of iterations between inviscid and boundary layer modules
41-50	XROUGH	-1.	Standard boundary layer calculation for smooth surfaces
		0.	Boundary layer calculation with area suction (needs cards 3 and 4)
		1.	Boundary layer calculation with surface roughness (needs cards 3 and 4)
51-60	REFC	arbitrary	Reference chord in inches for determination of surface distance in INSPAN

Column	Variable	Value	Description
61-70	UIN	arbitrary	Free-stream velocity in feet per second for use in INSPAN
71-80	XGEM	0.	Standard case; program will execute for complete case
		1.	Program will assemble and print out geometry variables only and stop

N.B.: REFC, UIN and XGEM currently not available.

Card 3 - Roughness Parameters

Column	Variable	Value	Description
1-10	UKU	30.-70.	Value of roughness Reynolds number where effect of roughness is independent of viscosity (see Ref. 1)
11-20	DEN	2.-100.	Density of roughness element spacing. (For sand grain roughness, use 3.175)
21-30	XO	.005-.02	Initial value of skin friction coefficient (.007 is usual starting value)
31-40	EPS	.0001	Error bound in skin friction calculation
41-50	XNROUGH	arbitrary	Number of input values of suction velocity, v_w/U, or roughness heights, k/c

Card 4 - Roughness or Suction Distribution

Column	Variable	Value	Description
1-10	VRD(1)	arbitrary (floating point)	Roughness height or area suction velocity (k/c or V/U_∞)
.	.		
.	.		
.	.		
61-70	VRD(NROUGH)	"	"

Card 5 - General Parameters

Column	Variable	Value	Description
1-10	XPRINT	0.	Suppresses printing of cross-flow integral thickness from IBL
		1.	Extra printing
11-20	XSKIP	1.	Print option in INTGRAL, every integration step is printed
		10.	Every tenth step is printed
21-30	REFX	arbitrary	Reference (x/c) location for calculation of moment coefficient
31-40	REFZ	"	Reference (z/c) location for calculation of moment coefficient
41-50	CREF	1.	Redundant
51-60	PRINT	0.	"
61-70	CASE	1.	Number of angle-of-attack or Mach number variations for a given geometry. Currently limited to 1

Card 6 - Variable Dimension Options

Column	Variable	Value	Description
1-5	NPANEL	.LE.1500	Number of source panels and vortex lattices on one side of plane of symmetry
6-10	NBX	2-70	Number of body sections
11-15	MBX	3-60	Maximum number of input points for any body section
16-20	NWX	2-40	Number of wing sections
21-25	MWX	3-59	Maximum number of ordinates at any wing section

Column	Variable	Value	Description
26-30	NVX	0-40	Number of streamwise vortices in body lattice
31-35	MVX	2-60	Number of bound vortices in body lattice
36-40	ILX	2-35	Sum of wing and body lattices
41-45	NPTS	.LE.1500	Number of off-body points

Geometry Input Cards - If the configuration is symmetrical about the x,z plane, geometrical input is required for only one side of the configuration. The convention used herein is to present that half of the configuration lying on the positive y side of the x,z plane. If the configuration is not symmetric, complete geometrical input is required.

Card 7 - General Identification - Card 7 contains any desired identifying information in Columns 1-80.

Column	Variable	Value	Description
10	CASE	1	Isolated body only
		2	Isolated wing only
		3	Wing-body combinations
20	PLOT	0	No plot output (currently this is the only option available)
		1	Plot output requested
30	SIM	0	Configuration symmetric about x,z plane; panel geometry required on one side only (normal case)
		1	Configuration symmetric about x,z plane. Panel geometry input required on one side only; panel geometry output calculated for both sides. (Used when analyzing symmetric configuration in yaw.) Not currently available
		-1	Asymmetric configuration. Panel geometry input required for both sides.

Column	Variable	Value	Description
40	ISAVE	0	Geometry and influence coefficient matrices not saved
		1	Geometry and influence coefficient matrices saved in previous run to be used (TAPE 11 must be requested). This option not yet checked out
		-1	Geometry and influence coefficient matrices to be saved on TAPE 11
50	PRINT	0	Normal output
		1	Optional output 1. Includes panel geometry, coordinate transformation matrices, and panel forces and moments
		2	Optional output 2. Panel velocity components and influence coefficients. Requires large line count limit
		3	Optional output 3. The aerodynamic influence coefficient matrix, the right side of the matrix equation, and all solution iterations
		4	Optional output 4. This option prints out the successive solution iterations only

N.B.: The normal output is always printed in addition to any optional output selected.

Card 9A - Single Panel Control Card

Column	Variable	Value	Description
1-10	SINGPA	0 1	No single panel input; omit card set 9B, continue reading input cards. Corner point coordinates of this panel follow on card set 9B
11-20	NOPAN	arbitrary integer	Number of panels to be deleted. If nonzero, panel indices follow on card set 9C

Card 9B - Panel Corner Point Input

Column	Variable	Value	Description
1-10	X(I)	arbitrary (floating point)	x-coordinate of corner I
11-20	Y(I)	"	y-coordinate of corner I
21-30	Z(I)	"	z-coordinate of corner I

Repeat card 9B four times, once for each corner of the panel.

Card Set 9C - Indices of Deleted Panels - NOPAN indices of deleted panels are read (7I10 format) if NOPAN > 0 on card 9A. A maximum of 100 panels may be deleted. Wing and body vortex lattice control panels may not be deleted.

Card Set 10 - Body Panel Input - This card set allows the body panels to be calculated automatically from the section geometry data. Five options are available for inputting the section geometry. The XYZ program input referred to below conforms with the format of Reference 2. Omit this card set if CASE = 2 on card 8.

Card 10A - Number of Body Sections

Column	Variable	Value	Description
1-10	NB	arbitrary integer	Number of body sections ($2 \leq NB \leq 70$)

Card 10B - Body Section Geometry

Column	Variable	Value	Description
1-10	XBE	arbitrary (floating point)	x-coordinate of origin of body section coordinate system, except blank when XYZ program input format is used
11-20	YBE	"	Similarly the y-coordinate
21-30	ZBE	"	Similarly the z-coordinate

Column	Variable	Value	Description
31-40	MB	arbitrary integer	Number of input points on section ($3 \leq MB \leq 60$);
			If MB < 0, XYZ program input format requested
50	OPT	0	Body section geometry input by y-z coordinates on card set 10C and 10D
		1	Body section beometry same as preceding body section - card set 10C or 10D omitted. Note: YBE and ZBE are additive to preceding values
		2	Body section geometry input in polar coordinates, r, θ, on card set 10C
		3	Body of revolution, section geometry input as section radius and theta increment on card set 10C
60	FLAG	0	Normal body section
		1	Terminal body section (end of current body panel network)
		2	End of rectangular grid

Card Set 10C - Body Section Coordinates (Normal Input)

Column	Variable	Value	Description
1-10	B(J)	arbitrary (floating point)	y-coordinate of point J if OPT = 0; or angular coordinate (in degrees) of J if OPT = 2; or increment angle, $\Delta\theta$, in degrees if OPT = 3
11-20	A(J)	"	z-coordinate of point J if OPT = 0; or r-coordinate of point J if OPT = 2; or body section radius if OPT = 3
21-30	D(J)	"	Δ x shift of point J if OPT = 0 or 2

Card set 10C contains MB cards if OPT = 0 or 2; contains only 1 card if OPT = 3; and is omitted if OPT = 1 or MB < 0 on card 10B.

Card Set 10D - Alternate ZYZ Input

Column	Variable	Value	Description
1-12	D(J)	arbitrary (floating point)	x-coordinate of point J
13-24	B(J)	"	y-coordinate of point J
25-36	A(J)	"	z-coordinate of point J

This card set is omitted unless MB < 0 in card 10B.

Note: Repeat card 10B and card sets 10C or 10D NB times to complete card set 10.

Card 11A - Number of Wing Sections

Column	Variable	Value	Description
1-10	NW	arbitrary integer	Number of wing sections ($2 \leq NW \leq 40$)
20	KOORD	1	Wing section ordinates input in percent of local chord
		2	Wing section ordinates input are not normalized

Card 11B - Wing Section Geometry

Column	Variable	Value	Description
1-10	XBE	arbitrary (floating point)	x-coordinate of origin of wing section coordinate system
11-20	YBE	"	Similarly the y-coordinate
21-30	ZBE	"	Similarly the z-coordinate
31-40	CHRD	"	Chord length section

Card 11B - Wing Section Geometry (continued)

Column	Variable	Value	Description
41-50	ALF	arbitrary (floating point)	Section twist angle (degrees) or flap rotation angle. (Degrees positive for positive flap deflection)
51-60	XAL	"	Center of twist or rotation in percent chord
61-65	MW	arbitrary integer	Number of coordinates in section ($5 \leq MW \leq 59$)
70	OPT	0	Wing section ordinates to be used from card set 11D
		1	Wing section ordinates same as preceding section - card set 11D omitted
75	FLAG	0	Normal case - surface vorticity calculated automatically
		1	Terminal wing section (end of current wing panel network)
		2	No vortex lattice panels calculated for this section
		3	The coordinates of the last bound vortex in the vortex lattice are read in on card 13 for this section
80	DEL	0	No wing dihedral
		1	Dihedral input on card set 11C

Card Set 11C - Wing Dihedral Input

Column	Variable	Value	Description
1-10	DELTA	arbitrary (floating point)	Dihedral angle (degrees)

Card Set 11C - Wing Dihedral Input (continued)

Column	Variable	Value	Description
11-20	YO	arbitrary (floating point)	y and z ordinates of axis of rotation of wing panel
21-30	ZO	"	

N.B.: Omit card set 11C if DEL = 0 in card 11B.

Card Set 11D - Wing Section Coordinates

Column	Variable	Value	Description
1-10	B(J)	arbitrary (floating point)	x-coordinate of point J
11-20	A(J)	"	z-coordinate of point J

N.B.: Card set 11D contains MW cards of OPT = 0, and is omitted if OPT = 1. Repeat card 11B and card sets 11C and 11D NW times to complete card set 11.

Card Set 12 - Vortex Lattice Control Point Location

Column	Variable	Value	Description
1-10	WAKE	arbitrary (floating point)	Extension of vortex lattice into wake in percent chord (usually 100.)
11-20	POINT	"	Location of vortex lattice control point in percent chord behind trailing-edge (usually .1)

N.B.: These values are not used if FLAG = 3 on card 11B.

Card Set 13 - Relocation of Vortex Lattice Terminal Points - This card set is omitted unless FLAG = 3 on card 11B. For each wing section having FLAG = 3, two additional cards are required to specify the terminal points of the streamwise vortices.

Card Set 13A - Inboard Terminal Points

Column	Variable	Value	Description
1-10	XLP	arbitrary (floating point)	x-coordinate of inboard edge of lattice terminal point
11-20	YLP	"	y-coordinate of inboard edge of lattice terminal point
21-30	ZLP	"	z-coordinate of inboard edge of lattice terminal point

Card Set 13B - Outboard Terminal Points - Same as card 13A for outboard edge of lattice terminal point.

Card Set 14 - Body Vortex Lattice Input - This card set allows additional vortex lattices to be located inside the body of wing-body combinations, and is omitted if CASE < 3 on card 8.

Card Set 14A - Number of Streamwise Vortices in Body Vortex-Lattice Network

Column	Variable	Value	Description
1-10	NV	arbitrary integer	Number of streamwise vortices in body vortex-lattice network (NV $\leq$ 40)

Note: The sum of all wing and body vortex-lattices may not exceed 35.

Card Set 14B - Vortex-Lattice Geometry

Column	Variable	Value	Description
1-10	XBE	arbitrary (floating point)	x-coordinate of origin of streamwise vortex
11-20	YBE	"	y-coordinate of origin of streamwise vortex
21-30	ZBE	"	z-coordinate of origin of streamwise vortex

Card Set 14B - Vortex-Lattice Geometry (continued)

Column	Variable	Value	Description
31-40	MV	arbitrary integer	Number of bound vortices in lattice $2 \leq MV \leq 60$
41-50	OPT	0	Vortex-lattice points to be read from card set 14C
		1	Vortex lattice points same as preceding. Omit card set 14C
		2	Optional vortex-lattice control panel coordinates read on card 14D3
51-60	FLAG	0	Normal case - vortex-lattice panels calculated
		1	Terminal vortex of current body vortex-lattice network
		2	Corner points of control point panel to be read on cards 14D2 and 14D3 (used when arbitrary control point is desired)
61-70	SIMPOT	0	Symmetry option specified on card 8 enforced for this vortex
		1	Symmetry option ignored for this vortex lattice (used for inserting vortex-lattice networks in vertical tails located in x,z plane)

Card Set 14C - Vortex-Lattice Coordinates

Column	Variable	Value	Description
1-10	B(J)	arbitrary (floating point)	x-coordinate of point J
11-20	A(J)	"	z-coordinate of point J
21-30	C(J)	"	Vortex-lattice strength at point J

Card Set 14C - Vortex-Lattice Coordinates (continued)

Column	Variable	Value	Description
31-40	D(J)	arbitrary (floating point)	Δy shift of point J

Card set 14C contains MV cards if OPT = 0, and is omitted if OPT = 1 on card 14B.

Control Set 14D - Vortex-Lattice Terminal Point and Control Point Coordinates
Two or three additional cards are required to specify the terminal point of the streamwise vortex, and the corner points of the lattice control point panel.

Card 14D1

Column	Variable	Value	Description
1-10	B	arbitrary (floating point)	x-coordinate of terminal point of streamwise vortex
11-20	A	"	z-coordinate of terminal point of streamwise vortex
21-30	D	"	Δy shift of terminal point of streamwise vortex

Note: This point also defines the upstream corner of the control point panel if FLAG $\neq$ 2 on card 14B.

Card 14D2 - Same as card 14D1, containing the coordinates of the downstream corner of the control point panel if FLAG $\neq$ 2 on card 14B. If FLAG = 2 on card 14B, this card contains the coordinates of the upstream corner of the control point panel.

Card 14D3 - If FLAG = 2 on card 14B, this card contains the coordinates of the downstream corner of the control point panel in the same format as card 14D1. Omit this card if FLAG $\neq$ 2 in card 14B1.

Note: Repeat card 14B and card sets 14C and 14D NV times to complete card set 14.

Aerodynamic Input Cards - The configuration panel geometry is transferred to the aerodynamic section of the program by TAPE 11. Additional aerodynamic input cards required are described below.

Card 15 - Case Identification Card - Card 15 contains any desired case identification in columns 1-80.

Card 16 - Iteration Option Card

Column	Variable	Value	Description
1-10	NIT	arbitrary integer	Maximum number of iterations (15 - 25)
11-20	IEPS	"	Exponent of 10 setting limiting value for residue of iterative solution (-3 or -4 recommended)
21-30	ITYPE	1	Blocked Jacobi iteration procedure
		2	Blocked Gauss-Siedel iteration procedure
		3	Blocked Gauss-Seidel with controlled successive over-relaxation
		4	Blocked Gauss-Seidel with successive over-relaxation

N.B.: Options 3 and 4 have not been completely checked out, but will be made available at a later date.

Card 17 - Configuration Options

Column	Variable	Value	Description
1-10	COMPT	0	Forces and moments calculated for complete configuration
		arbitrary integer	Forces and moments calculated on components. Panel indices of each component follow on card 26
11-20	SECT	0	No wing section forces and moments

Card 17 - Configuration Options (continued)

Column	Variable	Value	Description
11-20	SECT	1	Wing section forces and moments calculated. Wing section indices follow on card 25, panel indices in each section on card 26, and section reference lengths on card 29
		2	Forces and moments calculated on subsections. The number of subsections follow on card 25, the number of panel groups on card 27, the panel indices in each group on card 28, and subsection reference lengths on card 29

Card 18 - Reference Parameters

Column	Variable	Value	Description
1-10	REFA	arbitrary (fixed point)	Reference data
11-20	REFL	"	Reference chord (MAC)
21-30	XOO	"	Axial distance of leading-edge of MAC from origin
31-40	X25	"	Axial distance of quarter chord of MAC from origin

N.B.: Default option -- all variables set to 1. internally (leave card blank).

Card 19 - Configuration Lift Option

Column	Variable	Value	Description
1-10	KUT	0	Nonlifting configuration, no vortex-lattice Kutta condition imposed
		1	Lifting configuration, vortex-lattice Kutta condition imposed

Card 19 - Configuration Lift Option (continued)

Column	Variable	Value	Description
1-10	KUT	-1	Wing vortex lattice extends through body having same strength as adjacent wing vortex lattice
11-20	NBV	arbitrary integer	Number of body vortices (NBV $\leq$ 5)
21-30	NV(1)	"	Number of wing vortices associated with body vortex 1
31-40	NV(2)	"	Number of wing vortices associated with body vortex 2
.	.		
.	.		
.	.		
61-70	NV(5)	"	Number of wing vortices associated with body vortex 5

Card 20 - Compressibility Rule Option

Column	Variable	Value	Description
1-10	KOMPR	1	Gothert Rule 1 selected
		2	Gothert Rule 2 selected
11-20	POINTS	0	One body component case, no off-body points
		1	Flap case, off-body points will be calculated

Card 21 - Number of Mach Numbers

Column	Variable	Value	Description
1-10	NMA	arbitrary integer	Number of Mach numbers following on card set 22

Card 22 - Mach Number

Column	Variable	Value	Description
1-10	MA	arbitrary (floating point)	Mach number

Card 23 - Number of Angles-of-Attack and Yaw

Column	Variable	Value	Description
1-10	NAL	arbitrary integer	Number of angles-of-attack following on card set 24

Card 24 - Angle-of Attack and Yaw

Column	Variable	Value	Description
1-10	ALPHA	arbitrary (floating point)	Angle-of-attack in degrees
11-20	BETA	"	Angle of yaw in degrees

Card 25 - Number of Sections

Column	Variable	Value	Description
1-10	IS	arbitrary integer	Number of sections; omit if SECT = 0 on card 16

Card 26 - Panel Indices

Column	Variable	Value	Description
1-10	IA	arbitrary integer	Index of initial panel in section
11-20	IE	"	Index of final panel in section

Card 27 - Number of Panels in Subsections

Column	Variable	Value	Description
1-10	IREI	arbitrary integer	Number of panels in subsections. Omit if SECT < 2 on card 17

Card 28 - Subsection Panel Indices

Column	Variable	Value	Description
1-5	II(1)	arbitrary integer	Panel indices of all panels in subsection; omit if SECT < 2 on card 17
6-10	II(2)	"	
11-15	II(3) ... etc.		

Card 29 - Reference Lengths

Column	Variable	Value	Description
1-10	DELY	arbitrary integer	Width of section
11-20	REFL	"	Reference length of section
21-30	XLE	"	*Moment reference point of section*

N.B.: Cards 25 - 29 must be repeated for each angle-of-attack or yaw, if *section data requested.*

Streamline Input Cards - Each streamline selected is constrained to pass through a chosen panel. This avoids the possibility of the selected streamlines bunching together in the separated flow region.

Card 30 - Case Identification Card - Card 30 contains identification for the streamline calculations.

Card 31 - Streamline Option Card

Column	Variable	Value	Description
1-10	ENDFILE	-1	Program switches out of WBAERO onto the streamline overlay

Card 32 - Streamline Panel Selection

Column	Variable	Value	Description
1-5	NLIN	variable	Number of prescribed panels for streamline calculations
6-10	NSP(1)	variable	Panel number for streamline number 1
11-15	NSP(2)	"	Panel number for streamline number 2
16-20	NSP(3) ... etc.		

N.B.: Repeat this card TRMAX times.

Card 33 - End of Data - 6/7/8/9

PROGRAM OUTPUT DESCRIPTION

The standard output of the program is a function of iteration number as described in the following paragraphs.

In Iteration 1, tables of parameter values for variably dimensioned arrays from subroutines WBOLAY and WBPAN are printed out, followed by a table of panel corner points for the input geometry. Output from subroutine WBAERO is printed next; the list of variable dimensioned array parameters for this subroutine is followed by selected input parameters and a list of central processor times. The first time is at the entry point to the subroutine, and the difference between the second and third times gives the time to form the matrix of influence coefficients. The fourth time is printed just before entering the SOLVE subroutine, and the fifth time (after SOLVE) is printed out after SOLVE has given the history of the residual in the iterative solution method and the solved singularity strengths (in order of panel number).

The next table gives the attached flow velocity vector and magnitude and the pressure coefficient at each panel control point, and is followed by a summary of the total coefficients which include: the axial, normal and side forces; the moments about the coordinate axes; the pitching moment about the reference point and about the quarter chord of the MAC; the x-wise center of pressure; and the lift side force and drag coefficients.

All the following output is repeated for each iteration.

Output from the streamline program starts with the variable dimensioned array parameters. The prescribed streamline starting points and panels are given next followed by the tabulated characteristics for each streamline. The tables list the x,y,z coordinates, the velocity vector and magnitude, the pressure coefficient, the geodesic curvature (K_1, K_2), the metric coefficient (H_2) and the distance from the upstream end of the calculated streamline.

Next, the calculated boundary layer characteristics are tabulated for each streamline and include the local shape parameter and skin friction coefficient. Each table is preceded by a summary of the streamline geometry and pressure distribution.

Subroutine WAKECON output follows the boundary layer characteristics and starts with a summary of the separation points and the separation panels that give an approximate representation of the separation line. The geometric parameters for the separated-wake vorticity panels are then tabulated,

and are followed by the singularity strength solution: surface sources (sigma) and wake vorticity (gamma).

Tables of velocity and pressure coefficients in the presence of the separation model are the last output for each iteration. This output starts with the mean velocity (UM), the pressure coefficient (CP), and the wake total head decrement (DH) at the wake panel control points, and is followed by the surface velocity vector and magnitude and the pressure coefficient at each panel control point.

After the last iteration, the wetted area, the reference area, and the drag summary table are printed out; the table includes the drag coefficients for the skin friction, the pressure, and the total based on the reference area. The total drag is also presented in D/q form in the units of the reference area.

LIST OF SYMBOLS

A_{ij}	Aerodynamic influence coefficient
B_{ij}	Normal velocity due to external source
C_D	Total drag coefficient
$C_{D_{sy}}$	Profile drag coefficient (Squire and Young)
ΔC_{D_b}	Base pressure drag due to separation
C_L	Lift coefficient
C_M	Moment coefficient
C_f	Local skin friction coefficient
C_{D_f}	Skin friction drag
C_p	Pressure coefficient
C_τ	Shear stress integral
c	Chord
F, F_o, G, G_o	Universal functions in Curle's laminar method
g	Correction term to Thwaites' laminar method
H	Shape factor, ratio of displacement to momentum thickness (δ^*/θ)
K	Non-dimensional pressure gradient parameter
M	Mach number
M_L	Local Mach number

LIST OF SYMBOLS (Continued)

M_∞	Free stream Mach number
N	Number of singularities
n_i	Total normal velocity at i^{th} point
P	Static pressure, pounds per square inch absolute
R	Local radius of curvature
R_c	Chord Reynolds number $U_\infty c/\nu$
R_θ	Momentum thickness Reynolds number $U\theta/\nu$
$R_{\theta_{ins}}$	Streamwise momentum thickness Reynolds number at instability point
$R_{\theta_{trans}}$	Streamwise momentum thickness Reynolds number at transition
r	Transverse radius of curvature, inches
S	Distance along a streamline
U	Local velocity at edge of boundary layer
U_∞	Free stream velocity
u_τ	Friction velocity $(\tau_w/\rho)^{1/2}$
V	Tangential velocity at body surface
x,y,z	Cartesian coordinates of point
α	Angle-of-attack
β	Angle of yaw
γ	Vortex strength

LIST OF SYMBOLS (Continued)

δ	Boundary layer thickness
ρ	Density of air
σ	Source strength
τ	Shear stress
τ_w	Local surface shear stress

Subscripts

i	i^{th} value
in	Incompressible
ins	Instability
j	j^{th} value
L	Local Value
l	Lower
trans	Transition
t	Turbulent
u	Upper